External Tank (ET) Foam Thermal/Structural Analysis

July 27, 2006

TABLE OF CONTENTS

Volume I: Technical Consultation Report

1.0 Authorization and Notification 5
2.0 Signature Page 6
3.0 Team Members, Ex Officio Members, and Consultants 7
4.0 Executive Summary 8
5.0 Consultation Plan 9
6.0 Description of the Problem, Proposed Solutions, and Risk Assessment 10
6.1 Description of the Problem 10
6.2 Proposed Solution 10
6.3 Risk Assessment 10
7.0 Configurations Analyzed 11
7.1 Methodology 13
7.2 The Bipod Closeout Models 15
7.3 The IFR Precursor Models 26
7.4 The Detailed IFR Models 31
8.0 Findings, Recommendations, and Observations 62
9.0 Lessons Learned 64
10.0 Definition of Terms 64
11.0 Alternate View Point 64
12.0 List of Acronyms 65
Appendix A. ITA/I Request Form (NESC-PR-003-FM-01) 67
Appendix B. Foam Mechanical Properties 70

List of Figures

Figure 7.0-1. Bipod Closeout 11
Figure 7.0-2. LH_2 Ice/Frost Ramp 12
Figure 7.0-3. LO_2 Ice/Frost Ramps 12
STS-114 ET Separation Photograph 12
Figure 7.2-1. Bipod Closeout 15
Figure 7.2-2. Finite Element Mesh for the Two Bipod Closeout Models 16
Figure 7.2-3. Steady-State Temperature Profile Near Bipod Fitting 18
Figure 7.2-4 Bipod Closeout Model near the Bipod Fitting 19
Figure 7.2-5. σ_x in the Bipod Closeout BX-265 Foam (units of psi) 20
Figure 7.2-6. σ_y in the Bipod Closeout BX-265 Foam (units of psi) 20
Figure 7.2-7. σ_z in the Bipod Closeout BX-265 Foam (units of psi) 21
Figure 7.2-8. τ_{zx} in the Bipod Closeout BX-265 Foam (units of psi) 21
Figure 7.2-9. Steady-State Temperature for Interface Model 23
Figure 7.2-10. Foam Interface Model 24
Figure 7.2-11. Foam σ_x in the Interface Model (units of psi) 24

Figure 7.2-12. Foam σ_y in the Interface Model (units of psi) 25
Figure 7.2-13. Foam σ_z in the Interface Model (units of psi) 25
Figure 7.2-14. Foam τ_{zx} in the Interface Model (units of psi) 26
Figure 7.3-1. Initial IFR Redesign Concept 27
Figure 7.3-2. IFR Precursor Models 27
Figure 7.3-3. Thermal Profile in Ramp Model 28
Figure 7.3-4. Finite Element Mesh for IFR Precursor Models 28
Figure 7.3-5. Foam σ_x in the IFR Precursor Models (units of psi) 29
Figure 7.3-6. Foam σ_y in the IFR Precursor Models (units of psi) 30
Figure 7.3-7. Foam σ_z in the IFR Precursor Models (units of psi) 30
Figure 7.3-8. Foam τ_{yz} in the IFR Precursor Models (units of psi) 31
Figure 7.4-1. LO_2 IFR 32
Figure 7.4-2. LH_2 IFR Model 33
Figure 7.4-3. LO_2 IFR Model Substrate, Bracketry and NCFI 24-124 Foam 34
Figure 7.4-4. Complete LO_2 IFR Model 35
Figure 7.4-5. LH_2 IFR Substrate, NCFI 24-124 Foam, Insulators, and Al 2219 Bracket 36
Figure 7.4-6. PDL 1034 foam Fill Around Al Bracket Plus Hexcel F161-1581 Mounting Bracket 37
Figure 7.4-7. Complete LH_2 Ice/Frost Ramp Model 37
Figure 7.4-8. Temperature Profiles in LO_2 Model 39
Figure 7.4-9. LH_2 Ramp Temperature Profiles – Cold Case 41
Figure 7.4-10. LH_2 Ramp Temperature Profiles – Hot Case 42
Figure 7.4-11. LO_2 Ramp Model Sections 44
Figure 7.4-12. Foam σ_x in the LO_2 Ramp Model (units of psi) 45
Figure 7.4.13. Foam σ_y in the LO_2 Ramp Model (units of psi) 45
Figure 7.4-14. Foam σ_z in the LO_2 Ramp Model (units of psi) 46
Figure 7.4-15. Foam τ_{xy} in the LO_2 Ramp Model (units of psi) 46
Figure 7.4-16. Foam τ_{yz} in the LO_2 Ramp Model (units of psi) 47
Figure 7.4-17. Foam τ_{zx} in the LO_2 Ramp Model (units of psi) 47
Figure 7.4-18. Foam Normal Stresses in the LO_2 Ramp Model (units of psi) 48
Figure 7.4-19. Foam Shear Stresses in the LO_2 Ramp Model (units of psi) 49
Figure 7.4-20. Foam Normal Stresses in the LO_2 Ramp Model (units of psi) 50
Figure 7.4-21. Foam Shear Stresses in the LO_2 Ramp Model (units of psi) 51
Figure 7.4-22. LH_2 Ramp Model Sections 53
Figure 7.4-23. σ_x in the LH_2 Ramp Model (units of psi) 54
Figure 7.4.24. σ_y in the LH_2 Ramp Model (units of psi) 54
Figure 7.4-25. σ_z in the LH_2 Ramp Model (units of psi) 55
Figure 7.4-26. τ_{xy} in the LH_2 Ramp Model (units of psi) 55
Figure 7.4-27. τ_{yz} in the LH_2 Ramp Model (units of psi) 56
Figure 7.4-28. τ_{zx} in the LH_2 Ramp Model (units of psi) 56
Figure 7.4-30. Normal Stresses in the LH_2 Ramp Model (units of psi) 57

Figure 7.4-31. Shear Stresses in the LH_2 Ramp Model (units of psi)..... 58
Figure 7.4-32. Normal Stresses in the LH_2 Ramp Model (units of psi)..... 59
Figure 7.4-33. Shear Stresses in the LH_2 Ramp Model (units of psi)..... 60
Figure 7.4-34. ET-120 LH2 Ice/Frost Ramp Dissection Results..... 60

Volume I: Technical Consultation Report

1.0 Authorization and Notification

The request to conduct an assessment on the External Tank (ET) Foam Thermal Analysis Project was submitted to the NASA Engineering and Safety Center (NESC) on February 1, 2006.

The authority to proceed was approved in an out-of-board action on February 1, 2006. The NESC Review Board formally approved the project on March 10, 2006.

2.0 Signature Page

Assessment Team Members

Eugene K. Ungar, NESC Lead

Li C. Chang, GRC

Eric T. Malroy, JSC

David F. Moore, LaRC

Ryan A. Stephan, JSC

3.0 Team Members, Ex Officio Members, and Consultants

Eugene K. Ungar, NESC	Team Lead
Li C. Chang, GRC	Structural Analyst
Eric T. Malroy, JSC	Thermal and Fluids Analyst
David F. Moore, LaRC	Structural Analyst
Ryan A. Stephan, JSC	Thermal and Fluids Analyst
Ivatury S. Raju NESC	Structures Discipline Expert
Norman F. Knight GD	Structural Analyst
John Stadler, LaRC	Systems Engineering
Jaime Belitz, Swales, LaRC	Scheduler
Cindy Bruno, LaRC	Program Analyst
Stacey E. Walker, Swales, LaRC	Technical Writer

4.0 Executive Summary

An independent study was performed to assess the pre-launch thermally induced stresses in the Space Shuttle External Tank Bipod closeout and Ice/Frost ramps (IFRs). Finite element models with various levels of detail were built that included the three types of foam (BX-265, NCFI 24-124, and PDL 1034) and the underlying structure and bracketry. Temperature profiles generated by the thermal analyses were input to the structural models to calculate the stress levels. The analysis included both the thermally induced stress and the tank wall stress induced by the ET pressurization.

An area of high stress in the Bipod closeout was found along the aluminum tank wall near the phenolic insulator and along the phenolic insulator itself. This area of high stress might be prone to cracking and possible delamination.

There is a small region of slightly increased stress in the NCFI 24-124 foam near its joint with the Bipod closeout BX-265 foam. However, the presence of the interface does not substantially increase the thermally induced stress levels in the foam.

Removing the forward portion of the hydrogen tank IFR, leaving only the NCFI 24-124 acreage foam, would lower the thermally induced stresses in the NCFI 24-124 foam.

The IFR models indicated that the BX-265 foam mini-ramps do not increase the stress in the existing PDL 1034 foam in either the LO_2 IFRs or the LH_2 IFRs.

The highest calculated stresses in the BX-265 foam mini-ramps in both the LO_2 IFRs and the LH_2 IFRs are less than half the extreme values calculated in the Bipod closeout. Thus the mini-ramps are not highly stressed.

The calculated stresses in the NCFI 24-124 acreage foam are highest at the NCFI 24-124/PDL 1034/tank wall interface under the LO_2 and LH_2 IFRs. The highest calculated stresses in the LH_2 NCFI 24-124 foam are higher than in similar locations in the LO_2 IFR. This finding is consistent with the dissection results of IFRs on ET-120, which had been loaded twice with cryogenic propellant. Two of the three dissected LH_2 IFRs that were in locations with no protuberance aerodynamic load (PAL) ramp had cracks in the highly stressed areas of the NCFI 24-124 foam outboard of the cable tray. No cracks were found in any of the three LO_2 IFRS that were dissected.

5.0 Consultation Plan

This Charter establishes the Independent Thermal/Structural Analysis Team for ET Foam within the NESC. It defines the mission, responsibilities, membership, and conduct of operations for this assessment.

This assessment was initiated out-of-board by the authority of the NESC Deputy Director on February 1, 2006, and was formally approved by the NESC Review Board on March 10, 2006. The objective was to provide an independent assessment of the likelihood of creating thermally-induced cracks in the Shuttle's ET IFRs and Bipod foam closeout. Mitigators for the thermal stresses were identified.

An NESC team with relevant expertise was formed to perform the assessment. The team developed thermal and structural models of the oxygen IFRs, hydrogen IFRs, and Bipod foam. The team modeled the foam to identify areas of high stress concentration and assessed the propensity of cracking.

6.0 Description of the Problem, Proposed Solutions, and Risk Assessment

6.1 Description of the Problem

The probable underlying cause of the large foam loss from the LH_2 tank PAL ramp on STS-114 was thermally induced cracks and associated delaminations along the tank substrate[1]. Although the PAL ramp has been eliminated from the next flight of the Space Shuttle, there was concern that the Bipod closeout and the IFRs on the ET would be susceptible to similar cracks from thermally induced stress, which could lead to foam loss.

To address this issue, an independent assessment of pre-launch thermally induced stresses in the Bipod closeout and IFR foam was performed. The assessment used highly simplified precursor models, models where the configuration was simplified, and highly detailed models to identify and assess regions of high stress.

6.2 Proposed Solution

The analysis showed high thermal stresses in the Bipod closeout and in the NCFI 24-124 foam under the LH_2 IFRs. The high thermal stresses calculated for the Bipod closeout are inherent in a system where the warm Bipod fitting is, of necessity, very close to the cryogenic tank. The high thermal stresses in the LH_2 IFRs outboard of the cable trays arise from the PDL 1034/ NCFI 24-124 foam interface perpendicular to the tank wall. This configuration is also inherent in the foam-on-foam design of the IFRs. The high stress areas could be eliminated by redesigning the Bipod fitting attachment and the IFR foam, but this may not be practicable.

6.3 Risk Assessment

Barring a redesign of the Bipod fitting attachment and the IFR foam, the risk of foam loss during ascent that is caused by cracking and possible delamination at the high stress areas must be dealt with through a probabilistic risk assessment.

[1] STS-114/ET-121 Investigation PAL Ramp Team Report, report number 809-8561, Lockheed-Martin Michoud Space Systems.

7.0 Configurations Analyzed

Three areas where thermally induced cracking might is likely to prior to launch were addressed in the present work: the Bipod closeout, LH_2 IFRs, and LO_2 tank IFRs.

The Bipod closeout was redesigned prior to STS-114. The new closeout, which is also planned to be used on all future Space Shuttle flights, is shown in Figure 7.0-1. It is a hand-sprayed application of BX-265 foam[2] that abuts the machine-sprayed NCFI 24-124[3] foam on the LH_2 tank and Intertank and the previously manually applied BX-265 foam over the flange (as indicated by the dotted boundaries shown on Figure 7.0-1). The Bipod closeout was chosen to be analyzed for thermally induced stresses because it is fairly thick and abuts a foam with different mechanical properties.

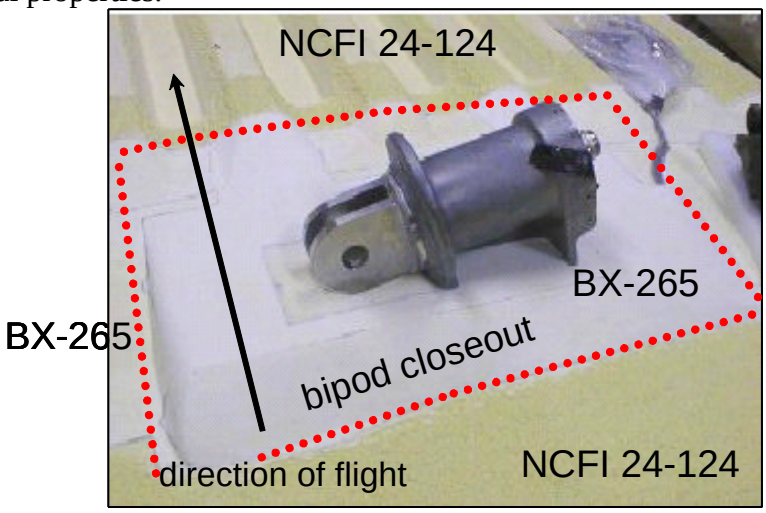

Figure 7.0-1. Bipod Closeout

The LH_2 IFRs prevent the formation of ice on the LH_2 tank cable tray and pressurization line support bracketry. A typical LH_2 IFR is shown in Figure 7.0-2. The IFRs are a poured PDL 1034[4] foam. Because of their thickness (a maximum of approximately 8 inches), and presence of an interface with the NCFI 24-124 foam, thermally induced cracking is a concern. In addition, in the areas where the LH_2 PAL ramp has been removed from existing ETs, a hand-sprayed BX-265 foam mini-ramp has been applied to maintain a uniform outer mold line for all of the LH_2 IFRs (see right side of Figure 7.0-2). The mini-ramp introduces a third foam in the IFRs, changes the thermally induced stress in that region, and may increase the probability of thermally-induced cracking.

[2] BX-265 is a hand-sprayed closed-cell polyurethane foam.
[3] NCFI 24-124 is a machine-sprayed closed-cell polyisocyanurate foam.
[4] PDL 1034 is a poured closed-cell polyurethane foam.

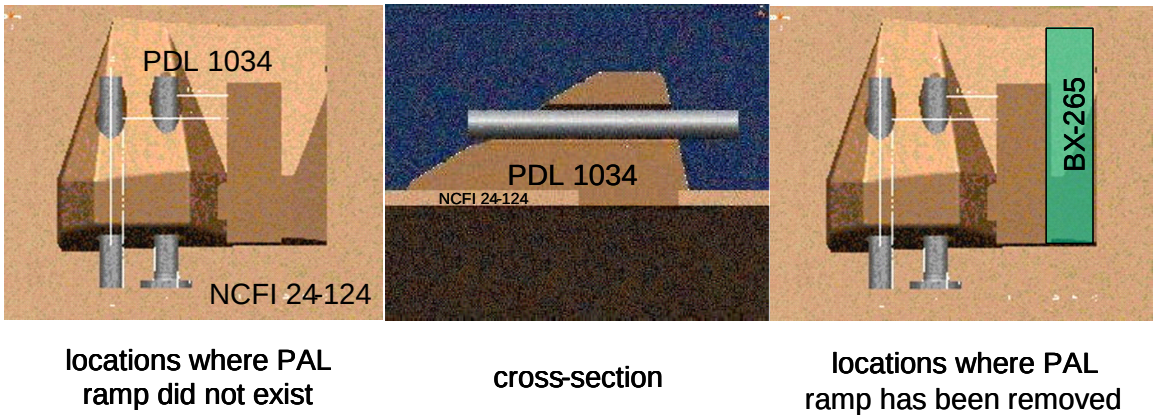

Figure 7.0-2. LH_2 Ice/Frost Ramp

The LO_2 IFRs prevent the formation of ice on the LO_2 tank cable tray and pressurization line support bracketry. These ramps are shown in Figure 7.0-3. The LO_2 IFRs are a poured PDL 1034 foam. They have a similar interface with the machine-sprayed NCFI 24-124 foam as the LH_2 IFRs, so thermally induced cracking is a concern here as well. In the areas where the LO_2 PAL ramp has been removed from existing ETs, a hand-sprayed BX-265 foam mini-ramp has been applied to maintain a uniform outer mold line for the IFRs. The new mini-ramp changes the thermally induced stress in this region and may increase the possibility of cracking.

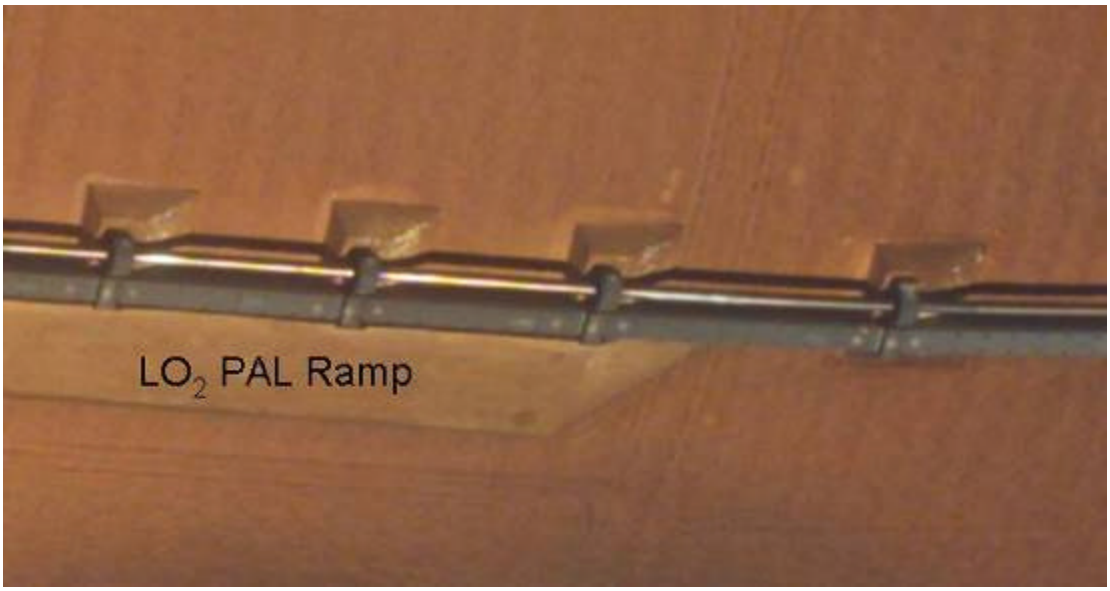

Figure 7.0-3. LO_2 Ice/Frost Ramps
STS-114 ET Separation Photograph

7.1 Methodology

Simplifications and Assumptions – Several simplifications and assumptions were made in the present work. Those specific to particular models are discussed in the appropriate section. The ones that apply globally are discussed here.

In all the models, the ET substrate was modeled as a flat plate. Because of the ET's 14-foot radius of curvature, even the widest model (at 34 inches) has a maximum deviation of less than ¾ inch from flat.

In all the models, the foams were assumed to have complete bonding with the tank substrate, the insulating blocks, bracketry, and with the other foams in the closeout. No voids or defects were assumed or included in these analysis models.

Foam Material Modeling - Cellular foam materials are difficult to model using the existing finite element technology. These foam materials exhibit inhomogeneity, anisotropy, nonlinearity, bimodular behavior, and temperature and strain-rate dependency. Inhomogeneity refers to the cellular nature of the foams and the lack of uniformity of the material due to the presence of knit lines and the non-uniformity of the foam cells. Anisotropy refers to having different material properties in different directions. Nonlinearity refers to the relationship between stress and strain, which usually is assumed to be linear. Bimodular behavior refers to the material exhibiting different behavior in tension and in compression. Temperature and strain-rate dependencies refer to the state dependencies of the material to temperature and the rate of strain.

Material data from the NASA/Marshall Space Flight Center database for foam materials present transversely isotropic tensile properties as a function of temperature. Transverse isotropy means the material properties in the longitudinal and circumferential directions are the same, while the properties in the thickness (or rise) direction are different.

In the finite element analyses reported here, the assumption was made that all foam behaves as a temperature dependent homogeneous linear elastic material with the same moduli in tension and compression. The mechanical property set used for each of the insulating foams is discussed in detail below.

NCFI 24-124 foam - two temperature dependent property sets are used: isotropic properties and transversely isotropic properties. For the latter, the properties in the foam rise direction differ from those in the directions parallel to the foam knit lines. Owing to the fact that the NCFI 24-124 foam is machine sprayed, the knit line orientation is consistent, facilitating the use of transversely isotropic properties. The foam rise direction is taken as perpendicular to the tank wall in all cases.

BX-265 foam – the knit lines in the BX-265 foam hand-sprayed applications analyzed in the present work are not consistently oriented with a single axis owing to their application techniques. Therefore, only the temperature dependent isotropic property set is used here.

PDL 1034 foam – the rise direction in the PDL 1034 foam poured applications analyzed in the present work are not consistently oriented with a single axis since the pours are made in a complex mold and must rise around pre-existing bracketry. Therefore, only the temperature dependent isotropic property set is used here.

The foam mechanical properties are listed in Appendix B. In addition, ultimate strength data for all three insulating foams is given for reference.

Modeling Technique – The thermal and structural models were developed and integrated in two different ways, depending on the complexity of the model. The configurations were simplified for all the models except the detailed models of the LO_2 and LH_2 IFRs. Here, separate thermal and structural models with identical configurations were developed using different analytical tools. The thermal model was solved for the steady-state temperature profile and that profile was used as input to the structural model. Only a single model was developed for each of the complex geometries of the LO_2 and LH_2 IFRs. These models were used for both the thermal analysis and, using the thermal analysis as input, for the structural analysis.

Stresses Analyzed – In the present work, the intensity of the stress state is characterized by examining the normal stresses and shear stresses. Because the calculated values of these parameters depend strongly on the material properties and assumptions used in the analysis (particularly the assumptions of homogeneity[5] and linear elastic behavior), the results must be interpreted with care. The stresses that are calculated by the current finite element models should be used for comparative purposes and not as quantitative measures. The strongest conclusions result from a one-to-one comparison of stresses in similar geometric configurations. Where similar configurations are not available for comparison, the values of the stresses within the model are evaluated to identify the areas of highest stress.

Orientation of the Coordinate System - All the results are reported with the coordinate system arranged so the tank longitudinal axis is along the x axis; y denotes the circumferential direction around the tank; and the direction perpendicular to the tank wall is z.

[5] Lack of sufficient data to characterize the influence of the inhomogeneity aspects of the foam preclude any assessment of their influence on the results presented.

7.2 The Bipod Closeout Models

Simplified models of the Bipod closeout region were developed to identify the areas of highest stress. The models were effectively two-dimensional, modeling an axial cross-section of the closeout as shown in Figure 7.2-1.

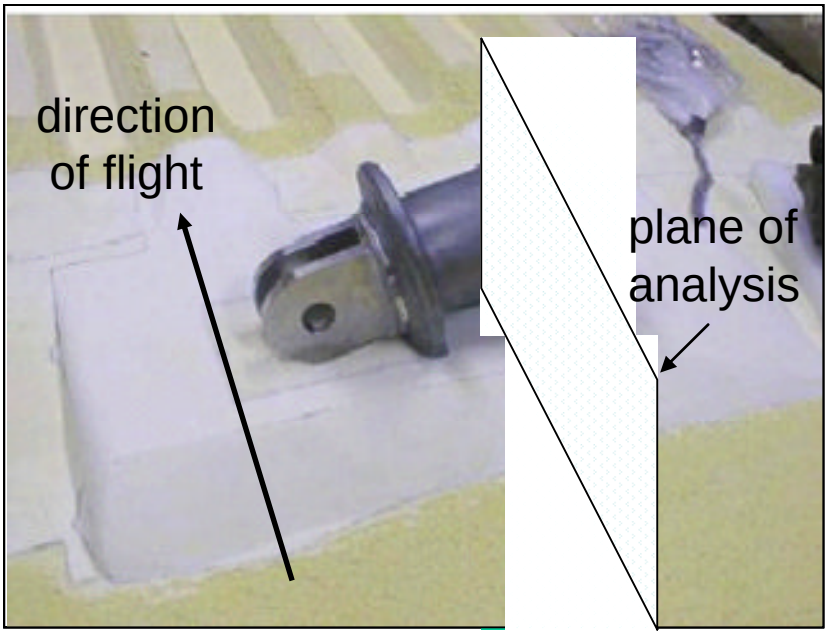

Figure 7.2-1. Bipod Closeout

Two models were built to investigate stresses near the Bipod fitting and at the BX-265/NCFI 24-124 foam interface. Figure 7.2-2 shows the configuration and the finite element meshes used in the models. The Bipod model on the left includes the Aluminum 2219 tank wall, A088 glass phenolic insulator that isolates the heated Bipod fitting from the tank, and representations of the copper Bipod fitting heater plate and the base of the Bipod fitting. The model is 6-inches wide, allowing essentially two-dimensional results to be obtained along its centerline. The foam interface model included the tank wall and two types of foam. The 10 by 10 inch ¼ inch thick 2219 Al baseplate is covered with a 1 inch thick layer of foam. The foam is evenly divided between BX-265 and NCFI 24-124 foams.

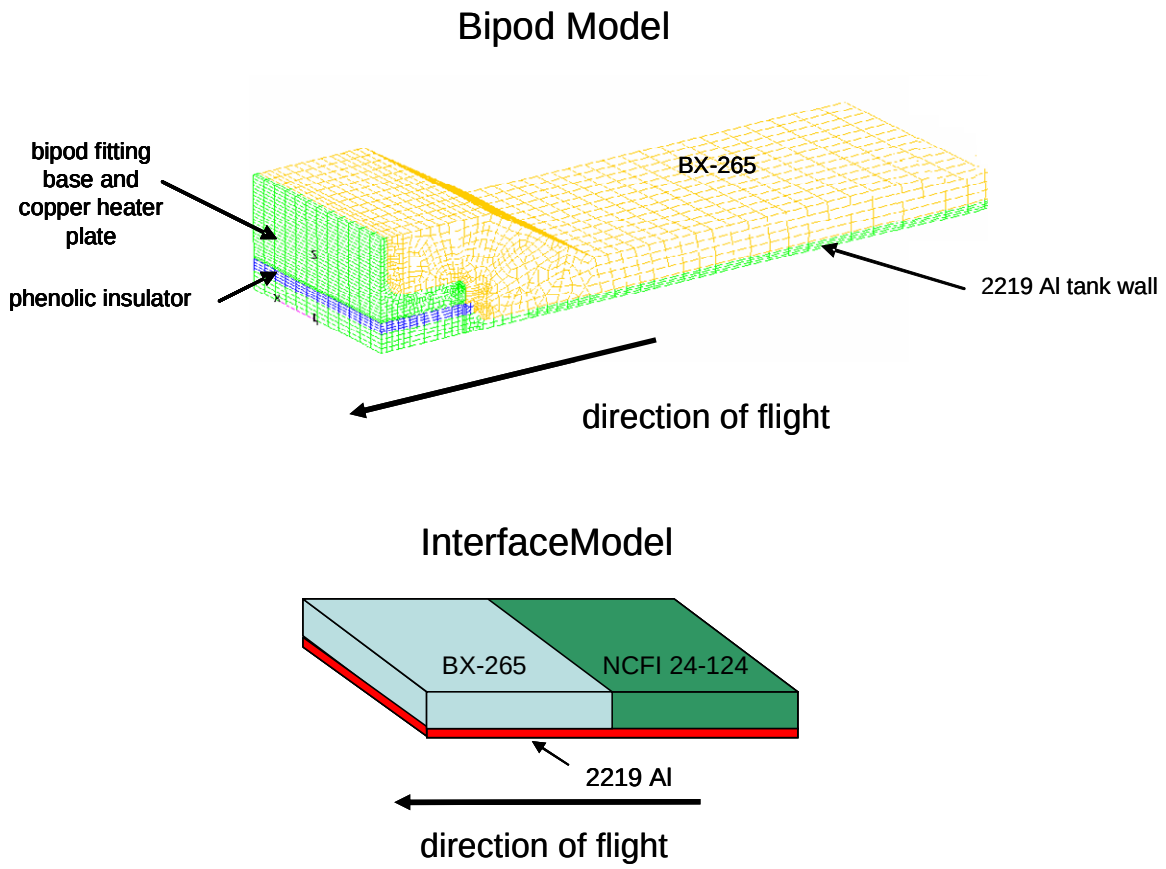

Figure 7.2-2. Finite Element Mesh for the Two Bipod Closeout Models

7.2.1 The Bipod Closeout Model

All dimensions used in the model were taken from the drawings for the ET. The thermal and structural models were geometrically identical.

Thermal Model – A two-dimensional thermal model of the Bipod closeout region was built in Thermal Desktop™[6] to analyze the steady-state temperature field. The following pre-launch boundary conditions were applied to the thermal model:

- Tank wall at -423°F
- Outer surface of all foam at 70°F
- Cut surfaces of the foam were adiabatic
- Bipod fitting and underlying copper plate were maintained at 70°F

[6] Thermal Desktop™ is a registered trademark of Cullimore and Ring Technologies, Littleton, CO.

The pre-launch foam surface temperature can be warmer or colder than the assumed 70°F depending on the ambient temperature and the local convection coefficient. The Bipod fitting is actually cooler than 70°F, but remains above freezing. However, since the critical temperature for thermal stresses is the -423°F liquid hydrogen temperature, these simplifications should have only a small effect on the high stress regions in the foam. Thus, the boundary conditions of uniform 70°F temperatures for the foam free boundary plus the Bipod fitting and underlying copper plate are a reasonable simplification for this analysis.

The thermal properties for all the materials in this and in the other the models developed in the present work were taken to be isotropic. The thermal properties used in the present work for non-metallic materials were obtained from the Lockheed-Martin Michoud Space Systems Database[7]. The metal thermal properties were obtained from standard references.

The predicted steady-state temperature profile near the Bipod fitting is shown in Figure 7.3-3. The figure shows that the heated Bipod fitting causes a large region of the foam to be maintained at 70°F. There is an area of large temperature gradients in the foam near the phenolic insulator where the temperature changes from 70 to -423°F across the 0.325 inch thick insulator.

[7] Non-metallic thermal conductivities were taken from External Tank Thermal Data Book 80900200102, Revision G, Lockheed-Martin Michoud Space Systems.

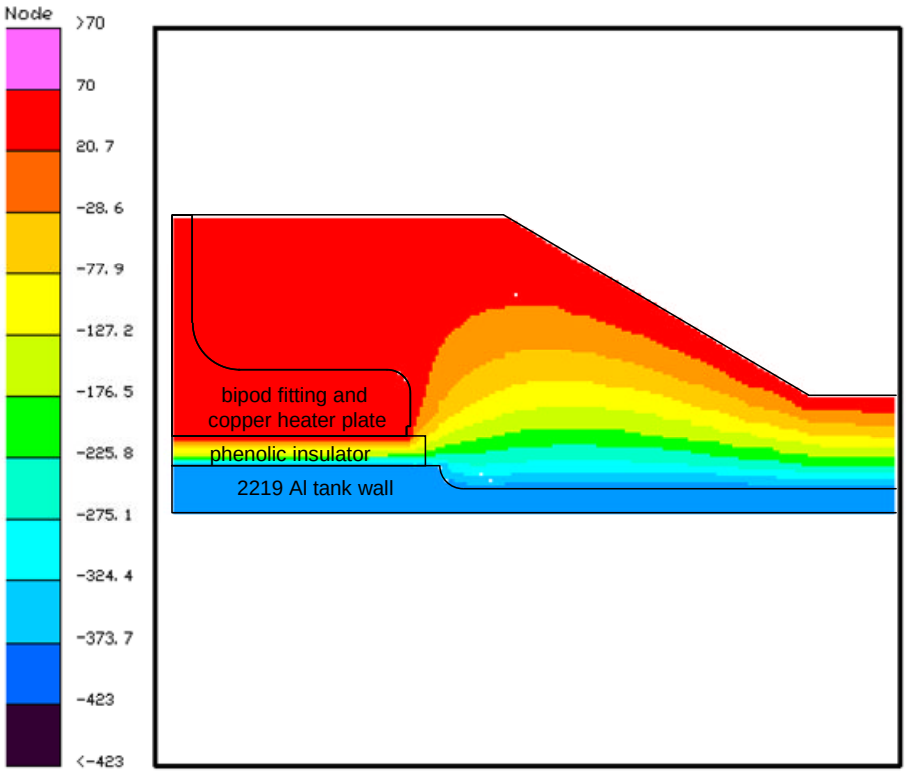

Figure 7.2-3. Steady-State Temperature Profile Near Bipod Fitting

Structural Results – The Bipod finite element model was built in the MSC.PATRAN™[8] interface to the NASTRAN™[9] structural analysis code. The model width was taken to be 6 inches, to yield essentially two-dimensional results along the model's plane of symmetry. The following boundary conditions were used:

- Reference temperature[10] of the materials is 75°F
- Applied temperature field per the thermal model results
- Tank wall was constrained to be flat
- Bipod fitting plane of symmetry (on the far left in Figure 7.2-3) was constrained to be flat and perpendicular to the tank wall

Aluminum 2219[11] mechanical properties were used for the Bipod fitting and the copper heater plate for convenience. Because this part of the model was held at a constant 70°F, the thermally

[8] MSC.PATRAN™ is a registered trademark of MSC.Software Corporation, Santa Ana, CA.
[9] NASTRAN™ is a registered trademark of NASA.
[10] The reference temperature is the temperature where there is zero thermal strain in the materials.

driven dimension change was negligible. In addition, because the titanium Bipod fitting and copper heater plate are both orders of magnitude stiffer than the foam[12], the analytical use of any metal's mechanical properties is acceptable here. The BX-265 foam was modeled as an isotropic material.

Figure 7.2-4 shows the material layout and the mesh used in the NASTRAN model. The mesh in the foam was refined at the location of maximum thermal gradients near the phenolic insulator and at the locations of complex geometries.

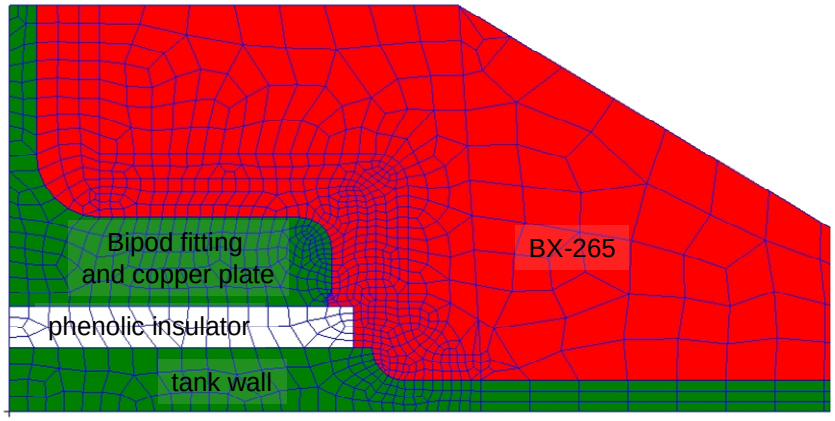

Figure 7.2-4 Bipod Closeout Model near the Bipod Fitting

Figures 7.2-5, 6, and 7 show the normal stresses in the foam on the plane of symmetry in the direction along the tank longitudinal axis, in the circumferential direction, and in the direction perpendicular to the tank wall, respectively. All three figures use the same fixed range scale for the stress level. Since the focus of the present work is the thermally induced stresses in the foam, only the foam stress is shown. Figure 7.2-8 shows the non-zero shear stresses in the foam on the centerline plane. Owing to symmetry, only τ_{zx} is non-zero.

[11] All metal structural properties were taken from: Sparks, Scotty, "BiPod Closeout ET Stress Report" LMMSS-ET-SEOS-439, January 23, 2006.
[12] Foam structural properties were taken from ET Project-Design Values for Non-Metallic Materials provided by the Lockheed Martin Space System in a test report "Contract NAS8-00016 WBS 3.6.1.7.2." – A listing of foam mechanical properties is contained in Appendix B.

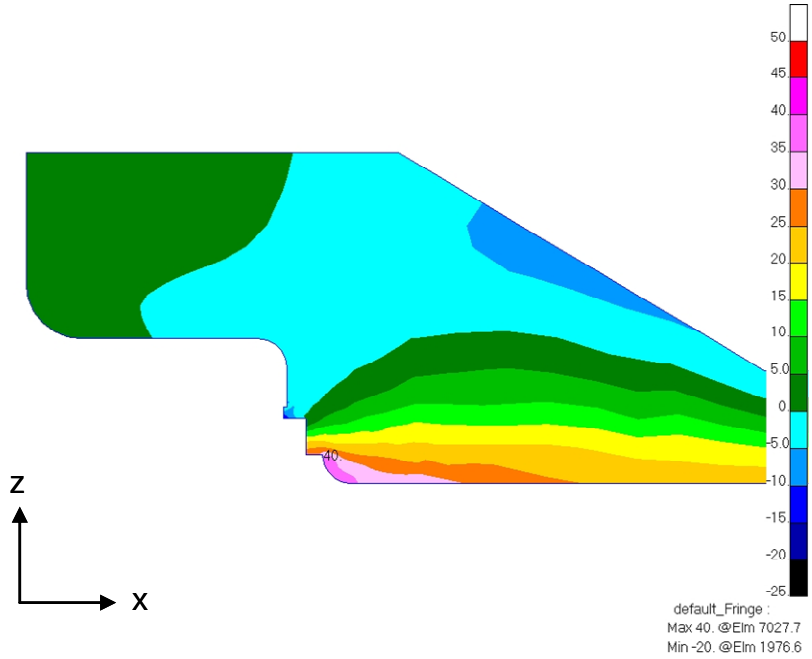

Figure 7.2-5. σ_x in the Bipod Closeout BX-265 Foam (units of psi)

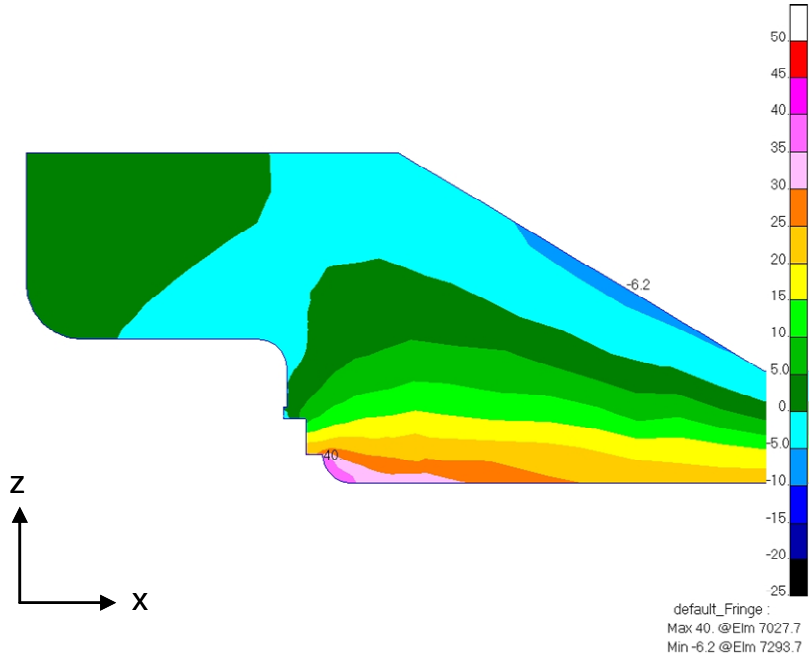

Figure 7.2-6. σ_y in the Bipod Closeout BX-265 Foam (units of psi)

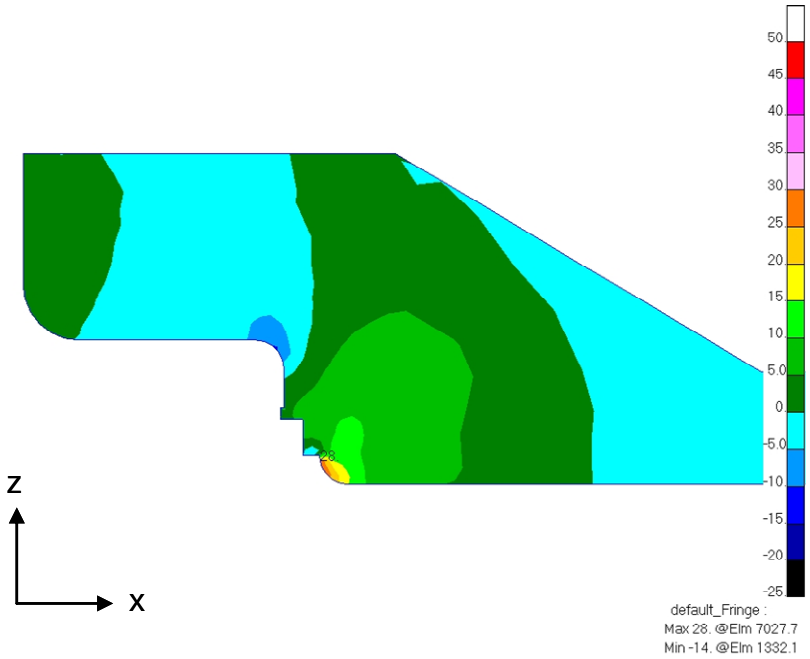

Figure 7.2-7. σ_z in the Bipod Closeout BX-265 Foam (units of psi)

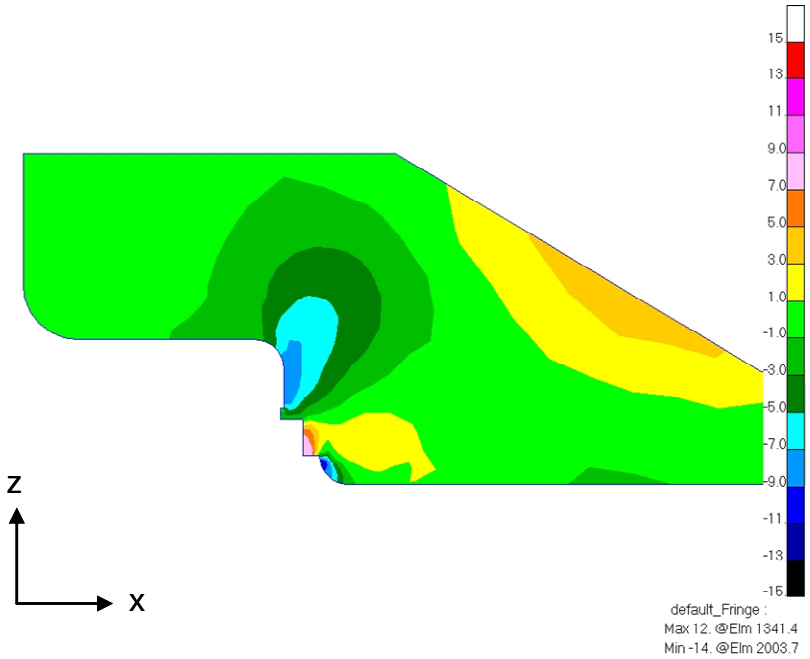

Figure 7.2-8. τ_{zx} in the Bipod Closeout BX-265 Foam (units of psi)

The Bipod closeout stress figures show a region of high tensile and shear stress located along the aluminum tank wall near the phenolic insulator and along the phenolic insulator itself. This area of high stress might be prone to cracking. In particular, the transverse normal stress σ_z exhibits a high local "peel" stress behavior near the interface. This result does not conflict with the dissection results from the Bipod foam qualification tests[13] and the dissection results[14] of the ET-120 Bipod closeout (ET-120 had been loaded twice with cryogenic fuel). The qualification test closeout showed no through cracking that was not associated with the details of the test configuration. The ET-120 dissection showed several through cracks in the Bipod closeout, although those cracks were not on the fitting centerline which is modeled here. The thermally induced stresses in those locations may have been exacerbated by three-dimensional effects in the closeout or the inhomogeneity and anisotropy of the foam material.

7.2.2 The Foam Interface Model

The foam interface model shown in Figure 7.2-2 was modeled a 10 by 10 inch piece of 1 inch thick foam on a 0.25 inch thick 2219 Al plate. The foam was half NCFI 24-124 foam and half BX-265 foam with an interface perpendicular to the plate.

Thermal Results – A two-dimensional thermal model of the interface was built in Thermal Desktop™ to solve for the temperature field. The following boundary conditions were used:

- Tank wall at -423°F
- Outer surface of all foam at 70°F
- Cut surfaces of the foam were adiabatic

The steady-state temperature profile for this model is shown in Figure 7.2-9. The slight unevenness in the temperature profiles at the center of the model is caused by the difference in thermal conductivities between the BX-265 and NCFI 24-124 foams.

[13] Kevin C. Davis External Tank Return to Flight Test Report 809-9486 Bipod TPS Thermal Vacuum Test Report, Lockheed-Martin Michoud Space Systems, February 19, 2005.
[14] MSFC Engineering Directorate M&P Laboratory, ET-120 & Related Dissection Summary, presented at MSFC Eng Assessment Team TIM 1/23/06.

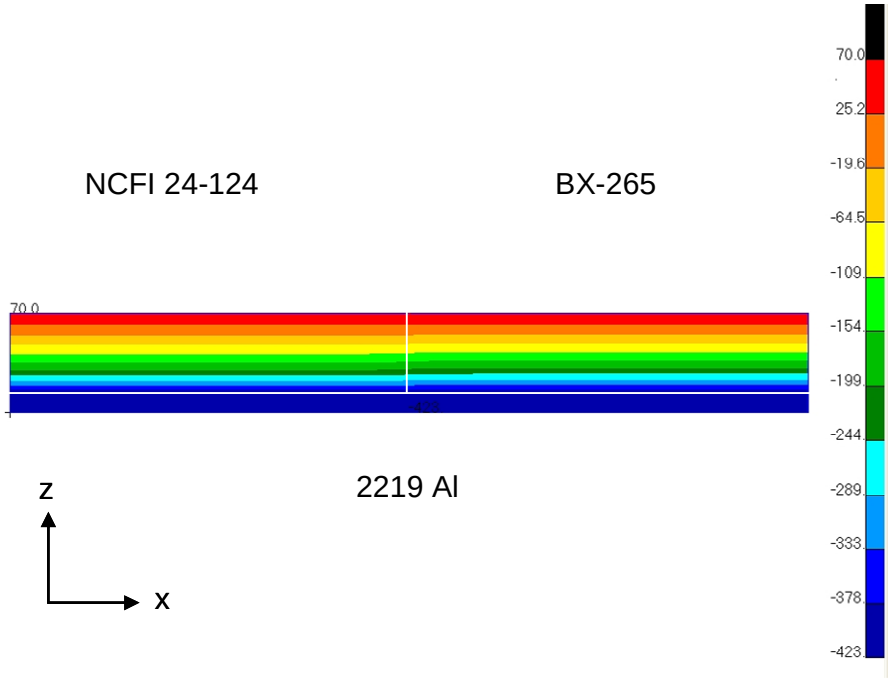

Figure 7.2-9. Steady-State Temperature for Interface Model

Structural Results – The finite element model for this case was built in the PATRAN interface to the NASTRAN structural analysis code. The structural model was run using the following boundary conditions:

- Reference temperature of the materials is 75°F
- Final temperature per the thermal model results
- 2219 Al was constrained to be flat

The BX-265 foam was modeled with isotropic properties. Transversely isotropic properties were used for the NCFI 24-124 foam. Figure 7.2-10 shows the material layout and finite element mesh in the model. The finite element mesh was defined so that the largest dimension of any element did not exceed 0.1 inch. The relative positions of the materials are maintained through the presentation and discussion of these results.

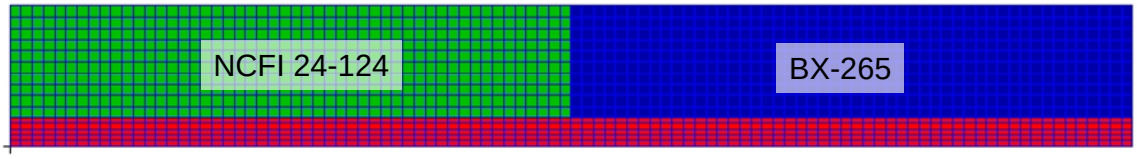

Figure 7.2-10. Foam Interface Model

Figures 7.2-11, 12, and 13 show the normal stresses in the foam calculated on the plane of symmetry in the direction along the tank longitudinal axis, in the circumferential direction, and in the direction perpendicular to the tank wall, respectively. All three figures use the same fixed range scale for the stress level. Figure 7.2-14 shows the non-zero foam shear stresses along the same plane.

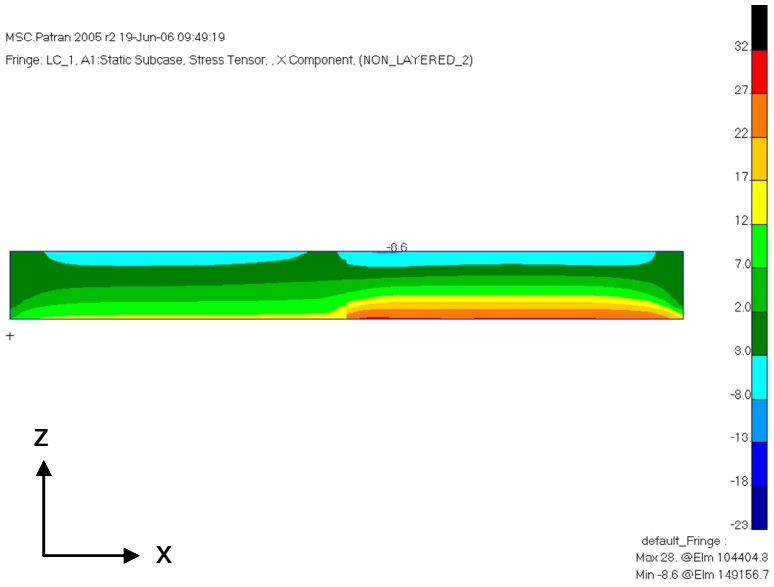

Figure 7.2-11. Foam σ_x in the Interface Model (units of psi)

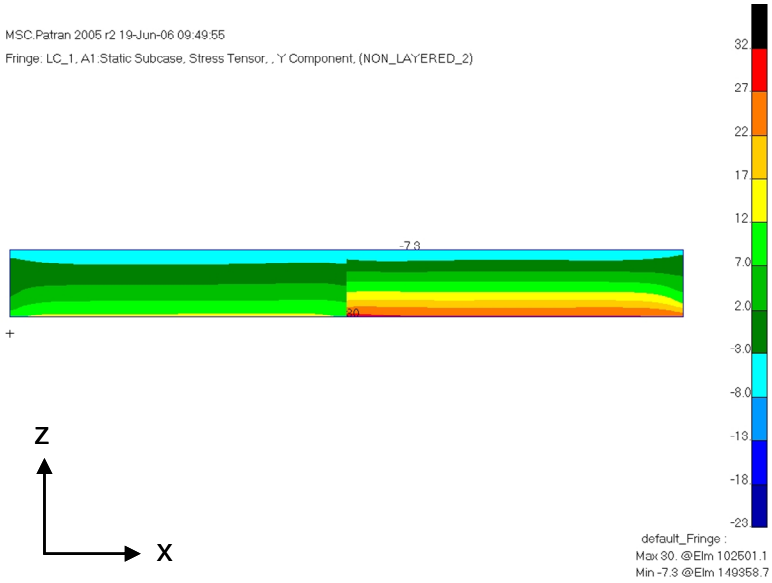

Figure 7.2-12. Foam σ_y in the Interface Model (units of psi)

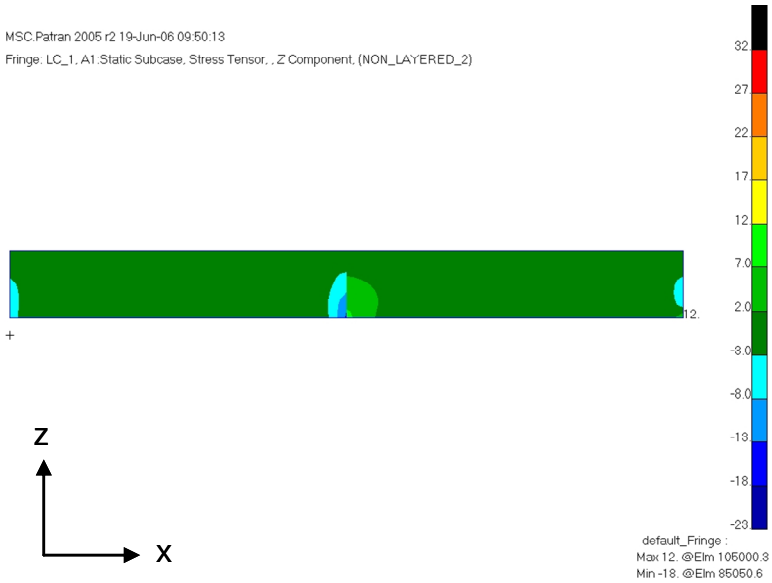

Figure 7.2-13. Foam σ_z in the Interface Model (units of psi)

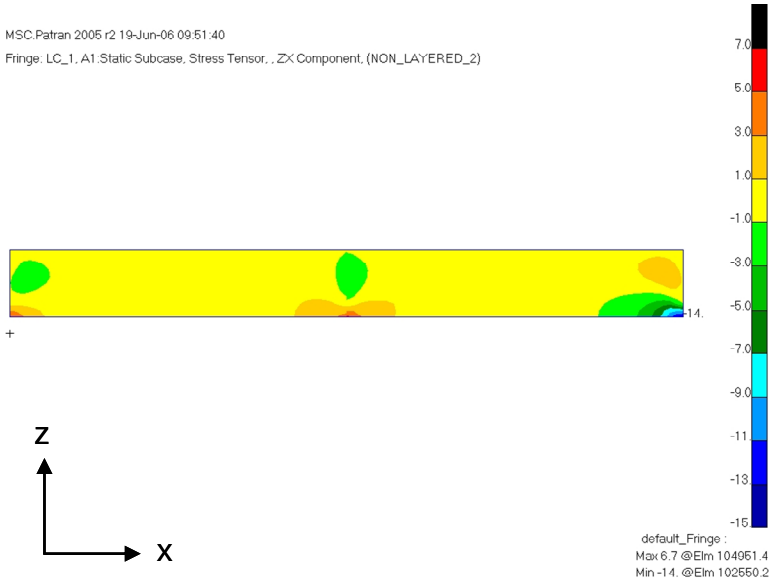

Figure 7.2-14. Foam τ_{zx} in the Interface Model (units of psi)

The figures indicate a small region of slightly increased stress in the NCFI 24-124 foam near the joint with BX-265 foam. Overall, however, the presence of the interface does not substantially increase the thermally induced stress levels in the foams.

7.3 The IFR Precursor Models

When the present work was begun, there was a plan to reduce thermal stresses in the LH_2 IFRs by removing the front part of the ramps (their "toes"). The planned flight configuration is shown in Figure 7.3-1. Two highly simplified models were built to provide a quick assessment of the effect of removing the IFR toe. One model was a simplified representation of the PDL 1034 foam ramp over machine-sprayed NCFI 24-124 foam. The second represented the NCFI 24-124 foam alone.

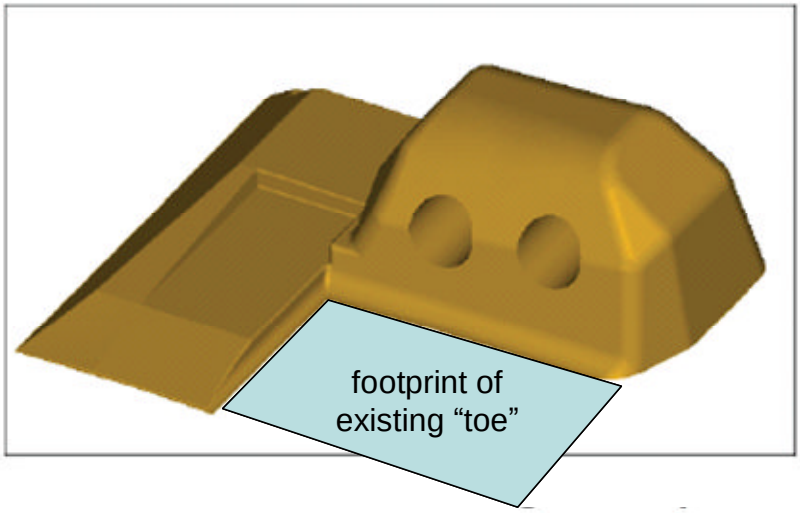

Figure 7.3-1. Initial IFR Redesign Concept

The geometries of these precursor models are shown in Figure 7.3-2. Both models include 1 inch of NCFI 24-124 foam on a 0.1 inch 2195 Al-Li plate. The ramp model has a 6 by 18 inch Al-Li baseplate. This model also includes a 6-inch wide by 4-inch tall ramp, representing approximately half the maximum IFR height. The no-ramp model has a 10 by 10 inch Al-Li baseplate.

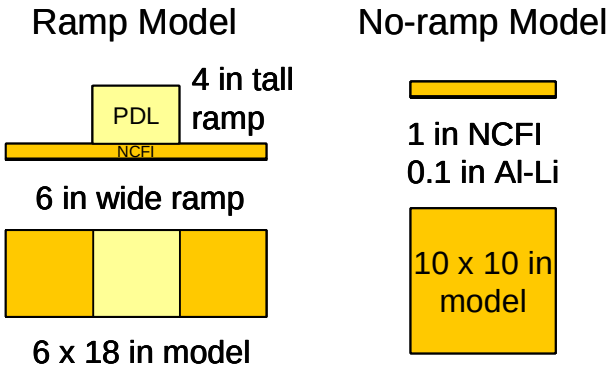

Figure 7.3-2. IFR Precursor Models

Thermal Results – Two-dimensional thermal models were built in Thermal Desktop to calculate the pre-launch thermal field in the foam. The following boundary conditions were used:

- Tank wall at -423°F
- Outer surface of foam at 70°F
- Cut surfaces of the foam were adiabatic

The thermal results of the ramp model are shown in Figure 7.3-3. The no-ramp model thermal results were identical to those shown on the left hand (NCFI 24-124) side of Figure 7.2-10 – the temperature field was one-dimensional, varying only through the thickness of the foam.

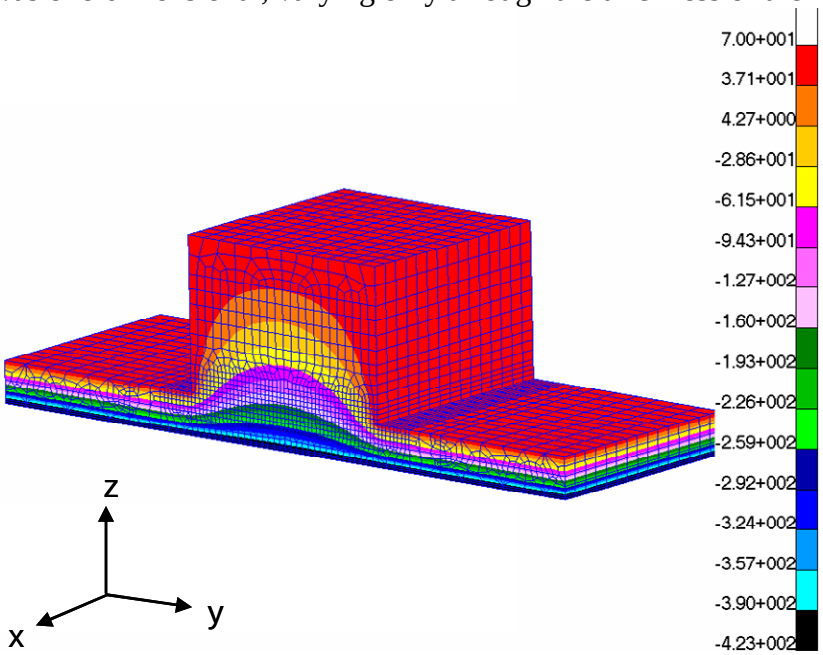

Figure 7.3-3. Thermal Profile in Ramp Model

Structural Results – The finite element IFR precursor models were built in the PATRAN interface to the NASTRAN structural analysis code. The finite element model is shown in Figure 7.3-4. As indicated in the figure, the finite element mesh is highly refined near the interface of the two foams in the Ramp Model.

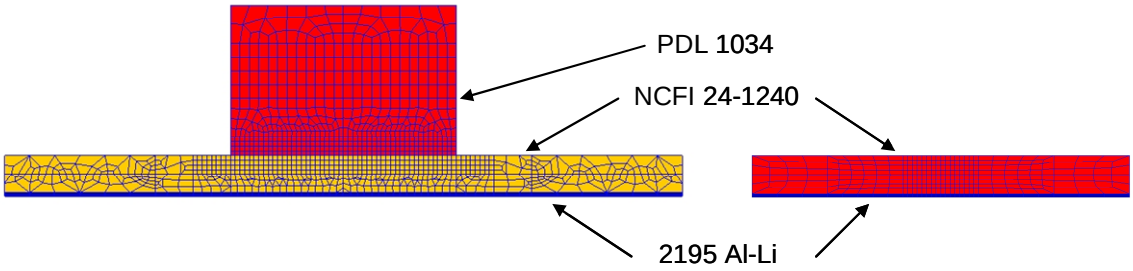

Figure 7.3-4. Finite Element Mesh for IFR Precursor Models

The following boundary conditions were used in the structural models:

- Reference temperature of the materials is 75°F

- Temperature distribution per the thermal model results
- Al-Li plates were constrained to be flat

The foams were modeled as isotropic materials.

Figure 7.3-5, 6, and 7 compare the foam normal stresses on planes cut through the model centers. All three figures use the same fixed range scale for the stress level. The foam non-zero shear stresses in the same locations are plotted in Figure 7.3-8. The stress contour plots are plotted by material property meaning that stress results for the same material property are smoothed across element boundaries and stress results for elements adjacent to each other with different material properties are not. Thus, a discontinuity in the stress results indicates a material property interface.

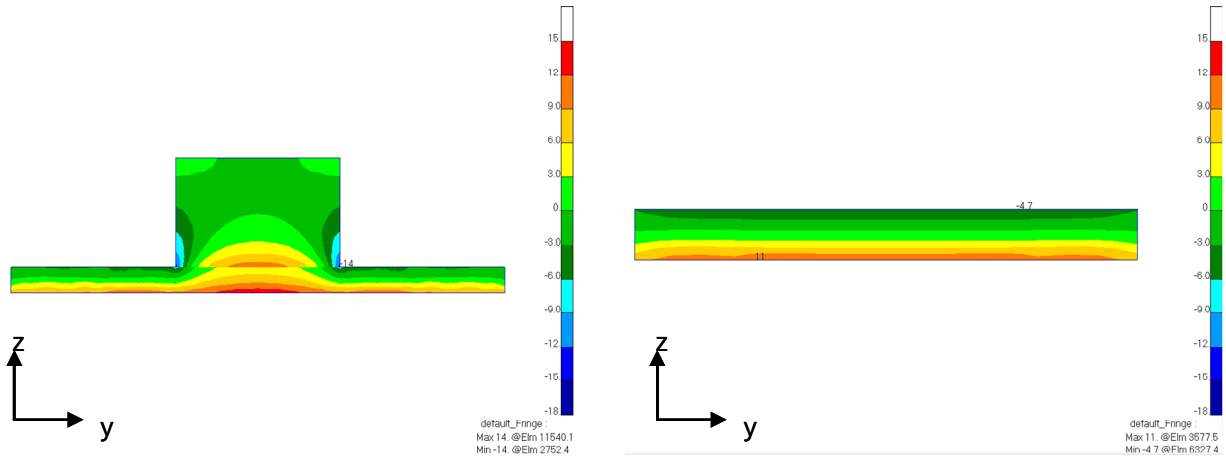

Figure 7.3-5. Foam σ_x in the IFR Precursor Models (units of psi)

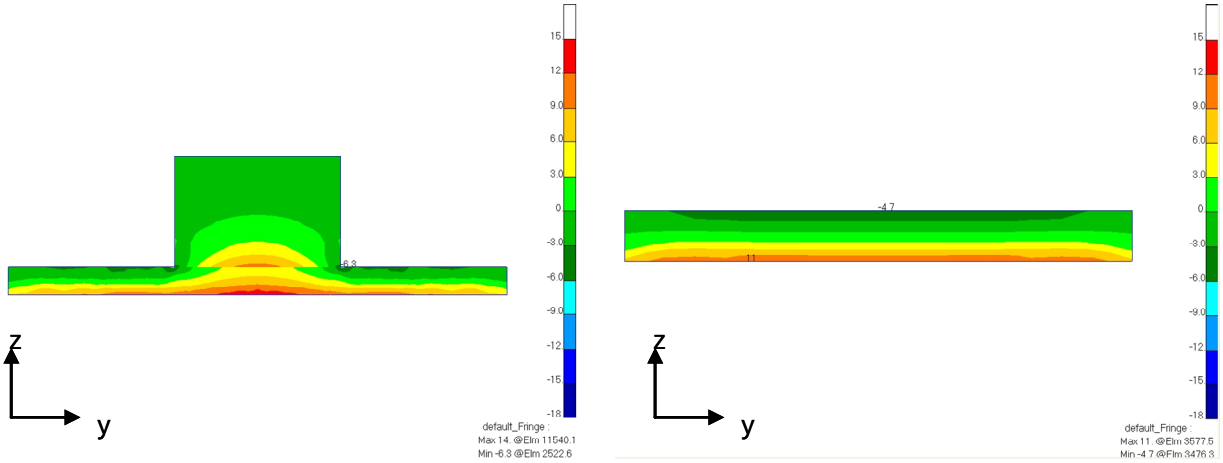

Figure 7.3-6. Foam σ_y in the IFR Precursor Models (units of psi)

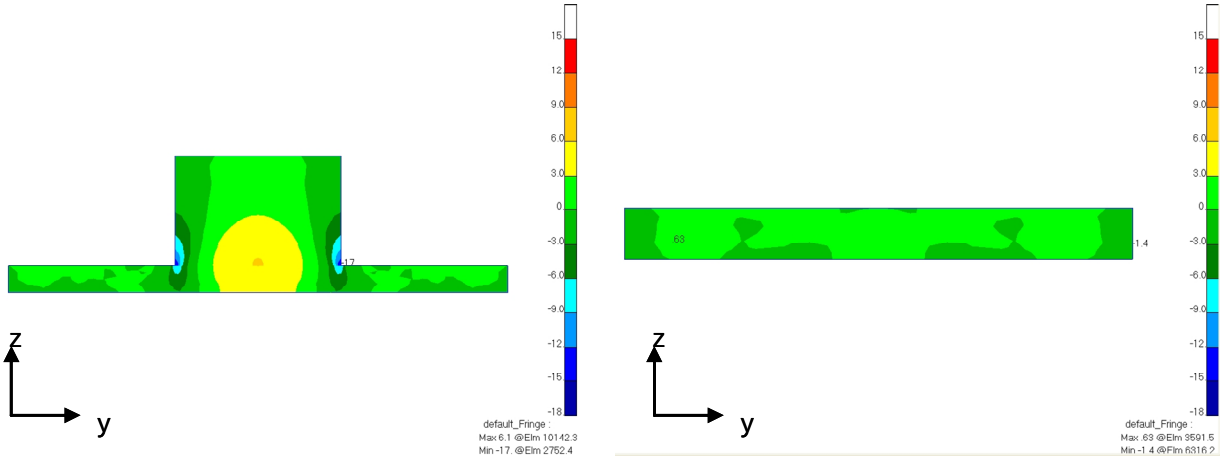

Figure 7.3-7. Foam σ_z in the IFR Precursor Models (units of psi)

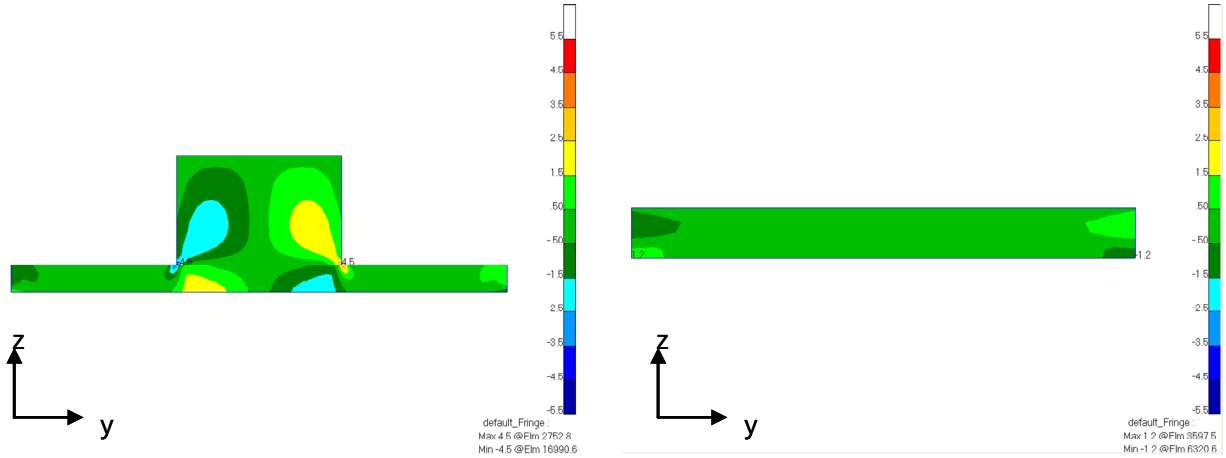

Figure 7.3-8. Foam τ_{yz} in the IFR Precursor Models (units of psi)

The figures show that the presence of the PDL 1034 foam IFR changes the stress distribution and significantly increases the stress in the NCFI 24-124 foam. In particular, a positive transverse normal stress (peel stress) is exhibited under the ramp as shown in Figure 7.3-7, which could contribute to delaminations.

The results of the LH_2 IFR precursor models indicate that removing the IFR toe, leaving only the NCFI 24-124 foam, would result in lower thermally induced stresses in the NCFI 24-124 foam. However, the degree of reduction in the stresses cannot be discerned from these models owing to their highly simplified nature.

7.4 The Detailed IFR Models

Two detailed IFR models were created in the present work, an LO_2 IFR model and an LH_2 IFR model. The models were designed to assess the thermally induced stresses in the ramps and to capture the stresses created by the BX-265 foam mini-ramps that replaced the LH_2 PAL ramp. The geometries of the two models were defined to be as simple as possible while maintaining sufficient detail to capture the thermally-induced stresses.

7.4.1 Methodology

LO_2 IFR Model - A LO_2 IFR is shown in Figure 7.4-1. The figure shows a plane of "symmetry" perpendicular to the tank wall that was used to simplify the modeling. The support bracketry and the PDL 1034 foam are nominally symmetric about the centerline of the IFR. In addition, the results[15] from thermal models of the IFRs developed by Lockheed-Martin Michoud indicate that the bracketry temperatures are also nominally symmetric about the centerline. Using the plane of symmetry to build the model in this way allowed the BX-265 foam mini-ramp and the

[15] External Tank Thermal Data Book 80900200102, Revision G, Lockheed-Martin Michoud Space Systems.

PDL 1034 foam that fills the same space at the non-PAL ramp locations to be assessed in the same model.

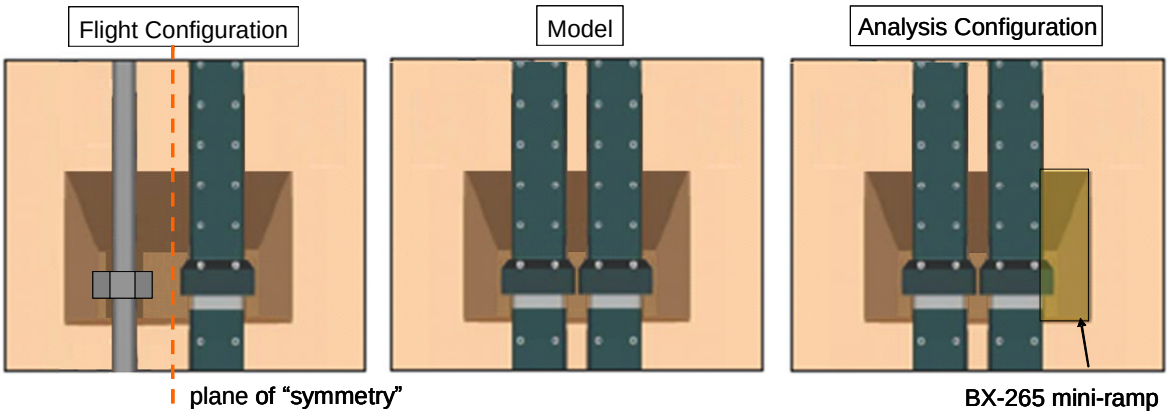

Figure 7.4-1. LO_2 IFR

The model was built using the configuration for the IFR at station 794 near the LO_2 tank/Intertank flange. The overall configuration of the IFR at this location is typical of the other LO_2 IFRs, but the details present a more severe case for the following reasons. The 1-inch thick NCFI 24-124 foam machine-sprayed foam at this location is the minimum thickness for LO_2 IFRs. This results in the coldest temperatures at the NCFI 24-124/PDL 1034 foam interface, yielding the highest thermal stress caused by differential thermal expansion. Also, the absence of super lightweight ablator (SLA) around the bracket at this location results a larger region of near-LO_2 temperature PDL 1034 foam, yielding the highest thermal stresses.

LH_2 IFR Model - The same symmetry technique was also used to build a model for the LH_2 IFRs. For this model, a similar plane of symmetry was identified at the inboard edge of the cable tray as shown in Figure 7.4-2. Even though this is not an exact plane of symmetry, the mini-ramp is far removed from this plane. Therefore, the thermally induced stresses near the BX-265 foam mini-ramp and the PDL 1034 foam that fills the same space at the non-PAL ramp locations is expected to be captured.

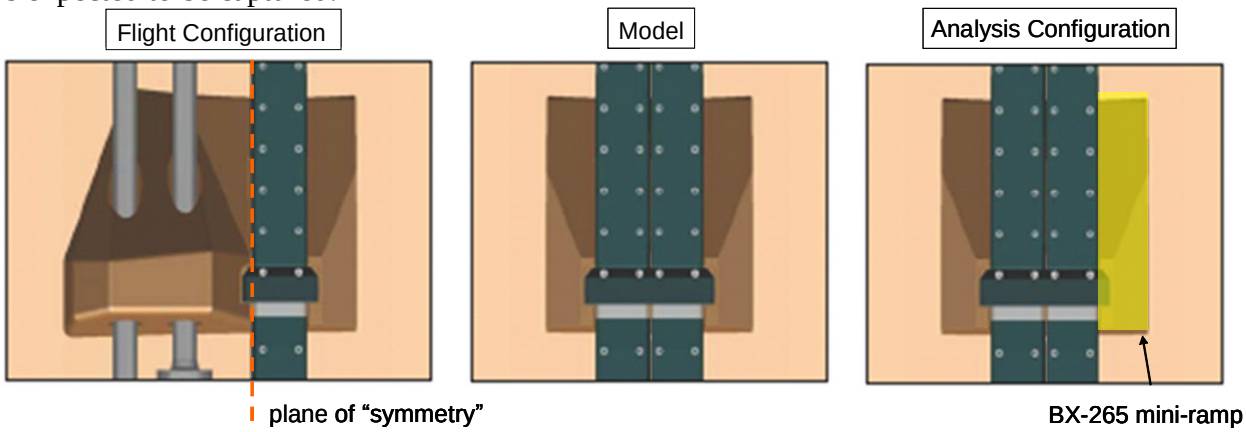

Figure 7.4-2. LH_2 IFR Model

The model was built using parameters for the IFR at station 1270 near the top of the LH_2 tank. The overall configuration of the IFR at this location is typical of the other LH_2 IFRs, but the ramp details present a more severe case for the following reasons. This location was chosen because it was the highest location with 1-inch (the thinnest application) of NCFI 24-124 foam machine-sprayed foam. Having a relatively thin layer of NCFI 24-124 foam results in the coldest temperatures at the NCFI 24-124/PDL 1034 foam interface and the highest thermal stress caused by differential thermal expansion. Additionally, the tank wall is thin-high on the tank. This maximizes the substrate strain in response to the tank pressurization that precedes LH_2 loading, creating the highest overall stresses in the foam near the tank wall.

Two significant simplifications were made in the configuration of the two IFR models:

- The 2219 Al and Hexcel F161-1581 bracketry was simplified by filling in webbed areas with the bracket material. For example, while the LH_2 aluminum cable tray mounting bracket is lightened by milling out the interior, a full thickness aluminum piece was modeled here. This is justified because bracket webbing affects only the temperature profile and should not affect the areas of high foam stress. Since the bracket temperature profile was used as input to the model, this simplification should not affect the stress results.
- The edges of the NCFI 24-124 foam around the mounting brackets was simplified in two ways to facilitate modeling. The rounded corners of the foam in both models and

the chamfer at the forward edge on the LO_2 tank foam were squared off in the models.

7.4.2 The Models

The two IFR models were built in PATRAN using similar techniques. The substrate, bracketry, and foam geometries were entered to create geometric shapes that were then meshed. The maximum dimension of any solid element in the models was ¼ inch. The models are discussed, in turn, in the subsequent sections.

LO_2 IFR Model – The bottom layer of the model is a 25 by 32 inch 2195 Al-Li plate whose thickness mimics the tank wall (the tank is thicker near the location of the brackets). The top of the plate is flat to facilitate modeling and changes in the plate thickness are accounted for on the bottom surface of the plate. The plate, 1-inch thick NCFI 24-124 foam, 2219 Al mounting brackets, and Hexcel F161-1581 laminate cable tray support are shown in Figure 7.4-3. Also indicated is the NCFI 24-124 foam pocket that is masked off during the machine-spray operation. The four corners of the pocket are rounded on the ET, but as mentioned above, are modeled as sharp corners. Also, the forward edge of the pocket on the ET is chamfered, but this feature is not modeled. The direction of flight is toward the lower right in the figure and in all subsequent isometric illustrations. The figure also shows the finite element model that was used in the analysis.

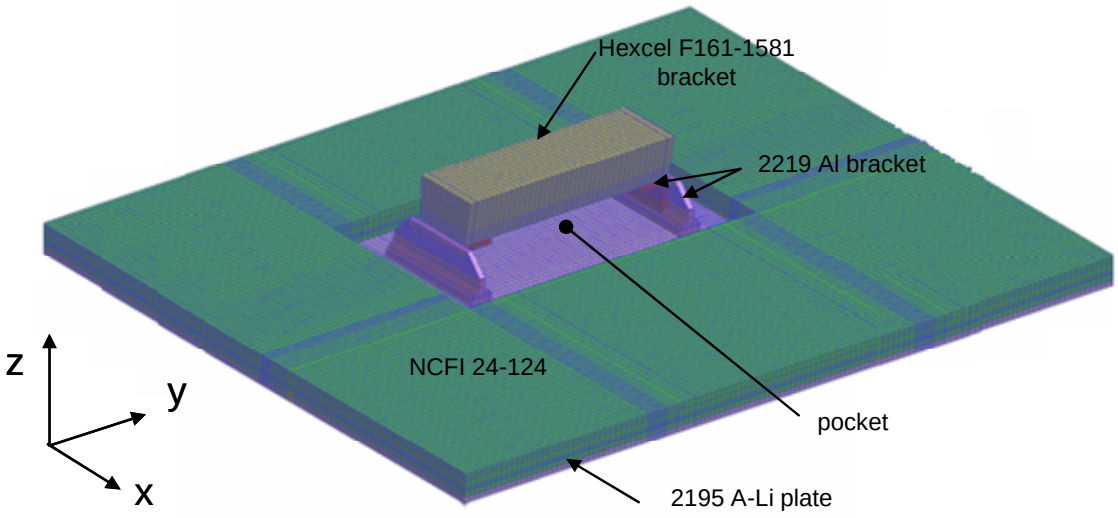

Figure 7.4-3. LO_2 IFR Model Substrate, Bracketry and NCFI 24-124 Foam

Figure 7.4-4 shows the outline of the complete model, i.e., the elements shown in Figure 7.4-3 with the PDL 1034 foam IFR and the BX-265 foam mini-ramp added.

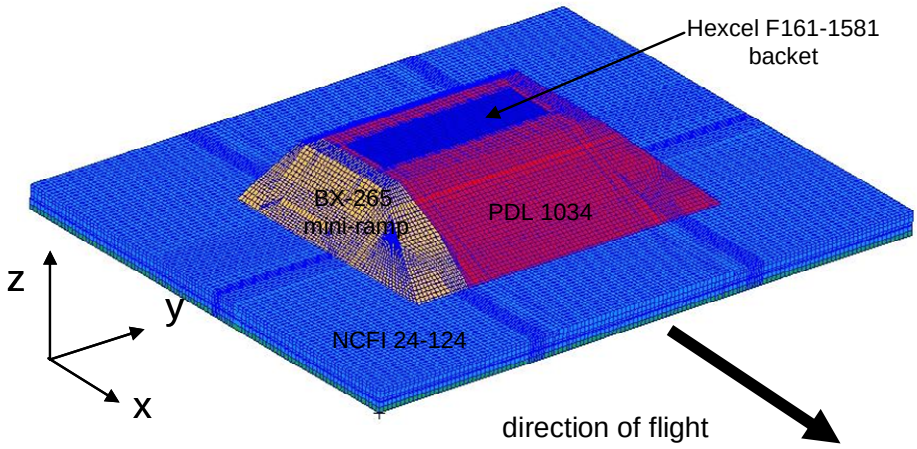

Figure 7.4-4. Complete LO_2 IFR Model

LH_2 IFR Model - The bottom layer of the model is a 34 by 29 inch flat 2195 Al-Li plate 0.1 inches thick, representative of the tank membrane thickness at Station 1270. The plate, 1 inch of NCFI 24-124 foam, phenolic insulators, and 2219 Al mounting bracket are shown in Figure 7.4-5. Also indicated is the NCFI 24-124 foam pocket that is masked off during the machine-spray operation. As in the LO_2 IFR model, the pocket corners which are rounded on the ET are modeled as square corners. The figure also shows the finite element mesh that was used in the analysis.

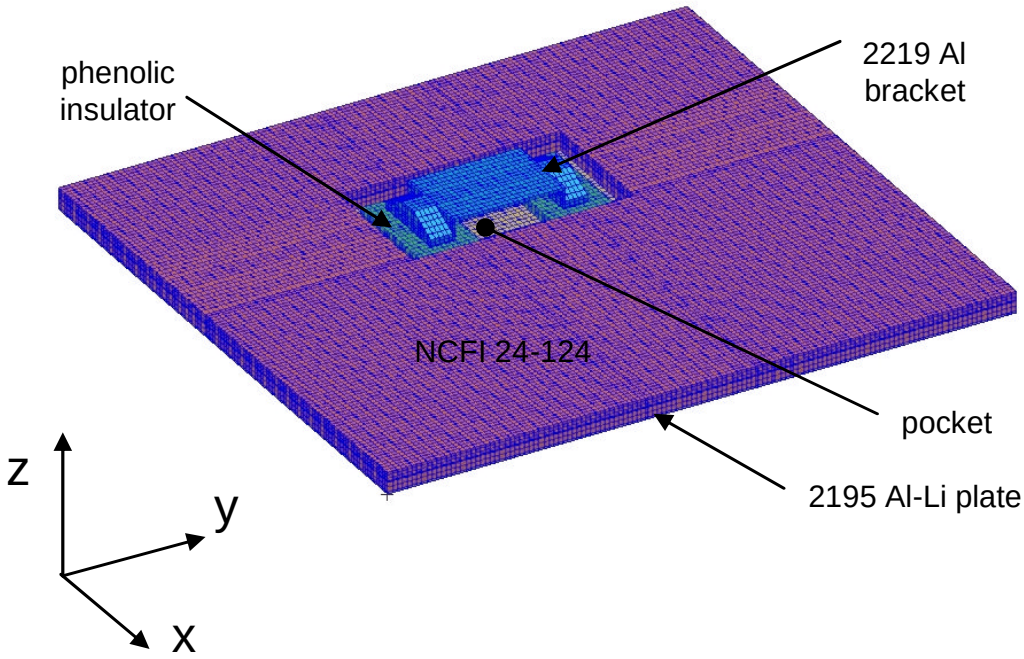

Figure 7.4-5. LH_2 IFR Substrate, NCFI 24-124 Foam, Insulators, and Al 2219 Bracket

Figure 7.4-6 shows the same configuration as in the previous figure with the addition of the Hexcel F161-1581 cable tray mounting bracket and the portion of the PDL 1034 foam that fills in the NCFI 24-124 foam pocket.

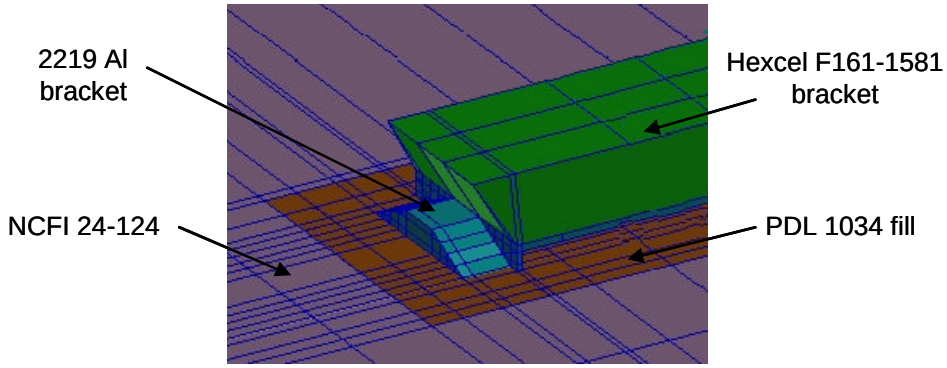

Figure 7.4-6. PDL 1034 foam Fill Around Al Bracket Plus Hexcel F161-1581 Mounting Bracket

Figure 7.4-7 shows the complete model. The top of the Hexcel bracket can be seen in line with the top surface of the PDL 1034 foam ramp.

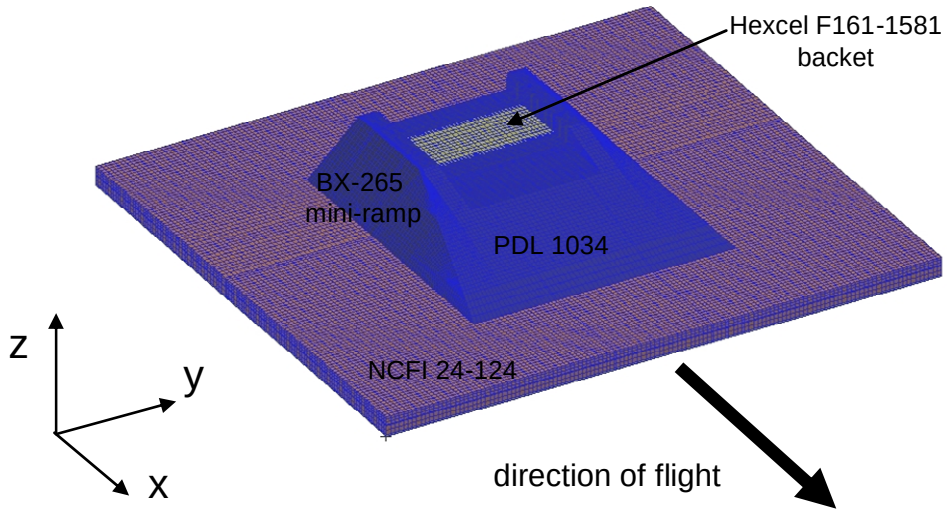

Figure 7.4-7. Complete LH_2 Ice/Frost Ramp Model

7.4.3 The Thermal Results

Similar pre-launch boundary conditions were used for the two detailed IFR models. The baseplate was held at the cryogen temperature, -297°F for the LO_2 model and -423°F for the LH_2 model. The cut surfaces of foam along the edges of the models were taken to be adiabatic. For

the LO_2 model, the temperatures of the Hexcel bracket were taken from Lockheed Martin Michoud minimum temperature predictions[16]. Results for two cases from the same source were used in the LH_2 cable tray model. Here maximum and minimum temperature predictions were used to set the temperatures of the aluminum bracket and Hexcel bracket. The boundary conditions of the foam exterior were taken to be consistent with the temperature predictions: for minimum temperature case, a cold ambient temperature of 31°F and a still air convection coefficient of 0.6 BTU/hr ft^2 °F[17] were applied; for maximum temperature case, an ambient temperature of 99°F and a 5 knot wind convection coefficient of 1.2 BTU/hr ft^2 °F were applied.

LO_2 IFR Model - The temperature distributions predicted by the LO_2 IFR model are shown in Figure 7.4-8. The figure shows the temperature on a plane cut through the center of the model along the tank axis and on a circumferential plane cut through the center of the bracket. The temperature profiles for all materials in the model are shown in the figures.

[16]External Tank Thermal Data Book 80900200102, Revision G, Lockheed-Martin Michoud Space Systems.
[17] Convection coefficients are calculated using HPSim Rev F, Lockheed Martin Michoud Space Systems.

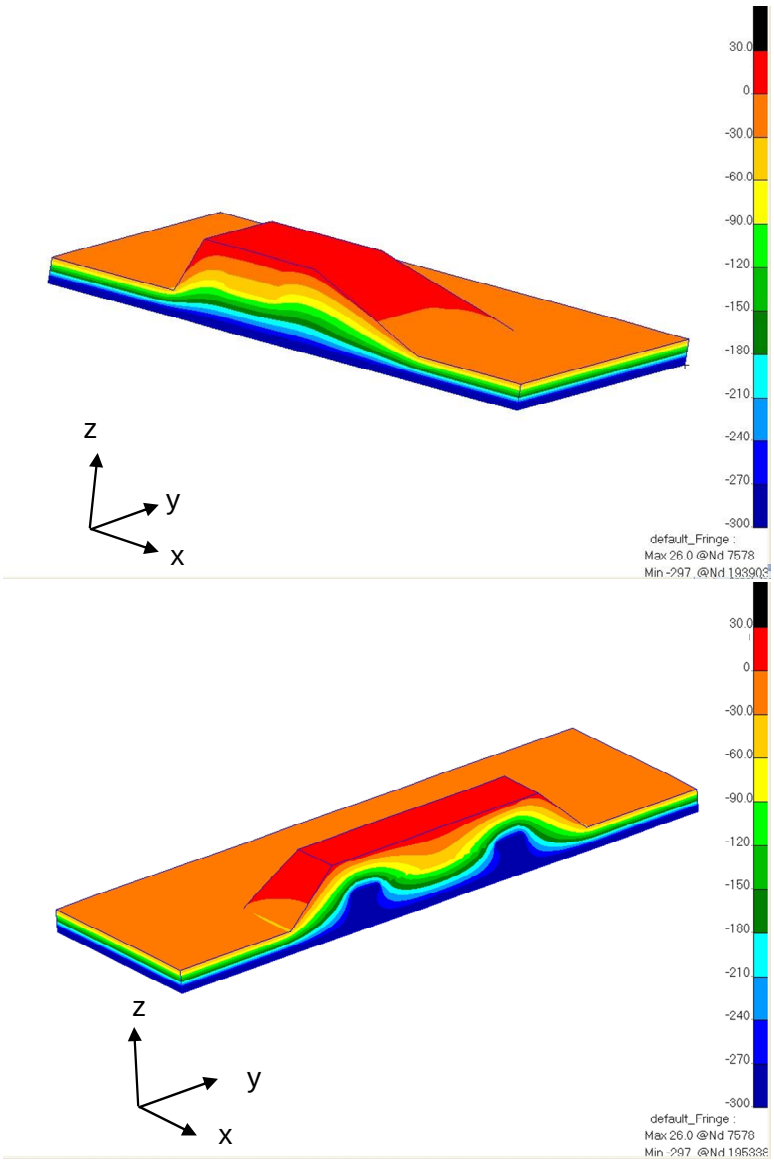

Figure 7.4-8. Temperature Profiles in LO_2 Model

The thermal results show the large low temperature area that is created by the 2219 Al mounting brackets. The figures also show that the presence of the ramp causes low temperatures to penetrate far into the insulating foam. This results in low temperatures at the NCFI 24-124/ PDL 1034 foam interface parallel to the tank.

LH_2 IFR Model - The temperatures predicted by the LH_2 IFR model are shown in Figures 7.4-9 and 10. Figure 7.4-9 shows the predicted temperature map for the minimum temperature (cold) case and Figure 7.4-10 shows the results for the maximum temperature (hot) case. The figures show the temperature on a plane cut through the center of the model along the tank axis, parallel plane cut through the bracket mount, and circumferential plane through the center of the bracket. The temperature profiles for all materials in the model are shown in the figures.

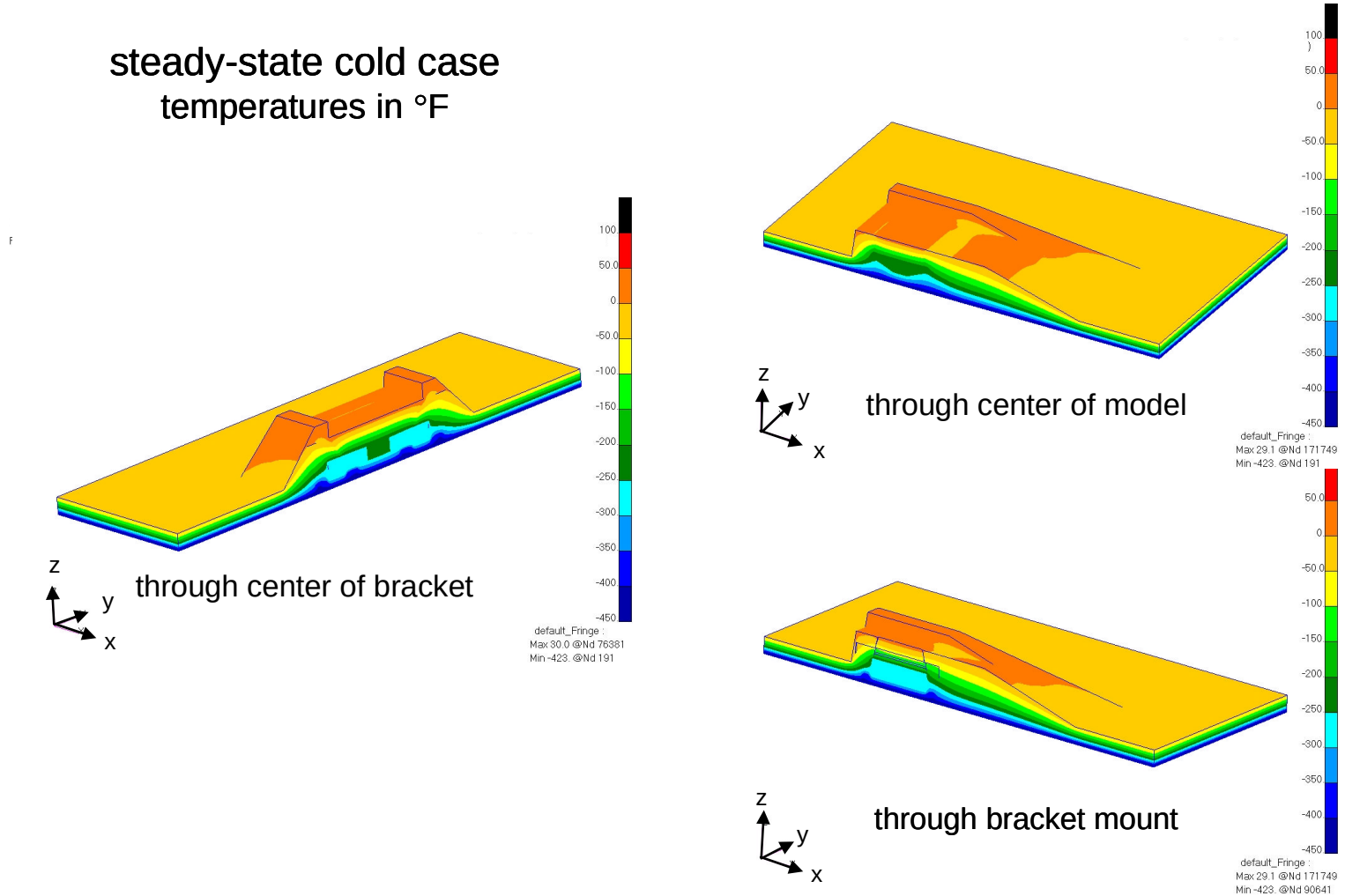

Figure 7.4-9. LH_2 Ramp Temperature Profiles – Cold Case

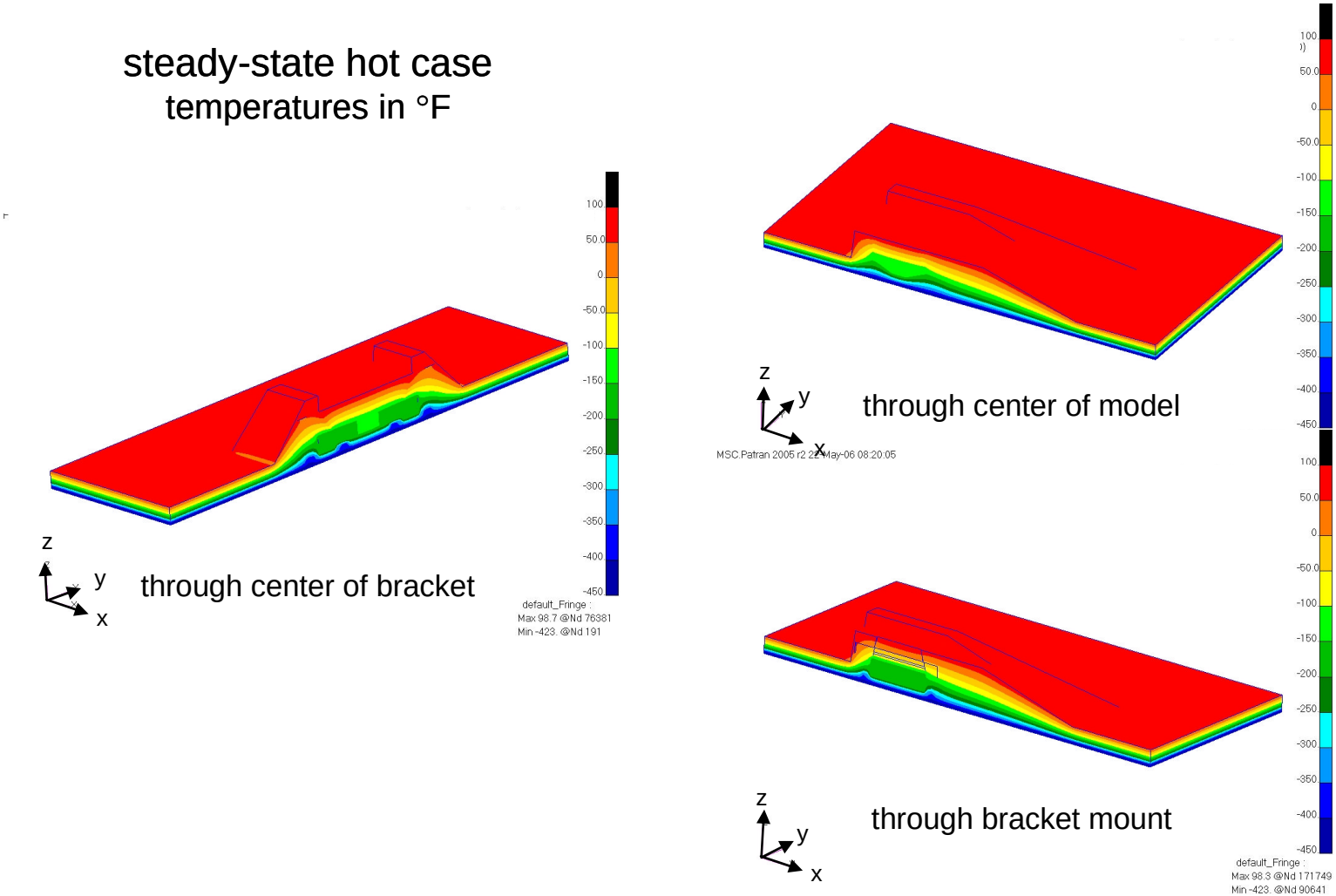

Figure 7.4-10. LH_2 Ramp Temperature Profiles – Hot Case

The thermal results show that the presence of the ramp causes low temperatures to penetrate far into the insulating foam. This results in low temperatures at the NCFI 24-124/PDL 1034 foam interface parallel to the tank.

7.4.4 The Structural Analysis Results

The boundary conditions for the stress analysis were consistent in the two IFR models. The temperature field calculated in the thermal models was applied to the structural models. For the cases with pressurization included, values of the hoop stress and axial stress were calculated to be applied uniformly over the appropriate edges of the tank substrate. The unpressurized cases had no applied stress at the substrate edges. As in the other models, the plates representing the tank substrate were constrained to be flat, but were allowed to expand and contract freely in-plane. The free edges of the NCFI 24-124 foam were not constrained.

LO_2 IFR Model - Three cases were run using the LO_2 IFR model. They were:

- isotropic properties for all materials
  - zero tank pressure
- transversely isotropic properties for NCFI 24-124 foam, isotropic properties for all other materials
  - zero tank pressure
  - 35 psig tank pressure[18] – the induced stress at the model edges was calculated based the tank pressure, the substrate thickness at the model edge, and the ET radius[19].

The results of the three cases were very similar. The choice of isotropic versus transversely isotropic properties had only a minor effect on the stresses in the NCFI 24-124 foam.

Figure 7.4-11 shows three sections that were cut through the model to facilitate presentation of the results. One section was cut along the circumferential plane through the center of the bracket. Two other sections were cut axially through the model, one through the model center, and the other through the bracket mount. The figure shows the model baseplate, bracketry, and three types of foam. The BX-265 foam mini-ramp is on the left of the figure.

[18] The oxygen tank is pressurized to 20 psig 2 minutes 55 seconds prior to launch, the hydrostatic head adds an additional 15 psig to the pressure at Station 794.

[19] At Station 794 the tank thickness is 0.184 inches at the locations corresponding to the edges of the model. The hoop stress owing to 35 psig on the 13.8 ft radius tank is 31,500 psi. The axial stress for the same condition is 15,700 psi.

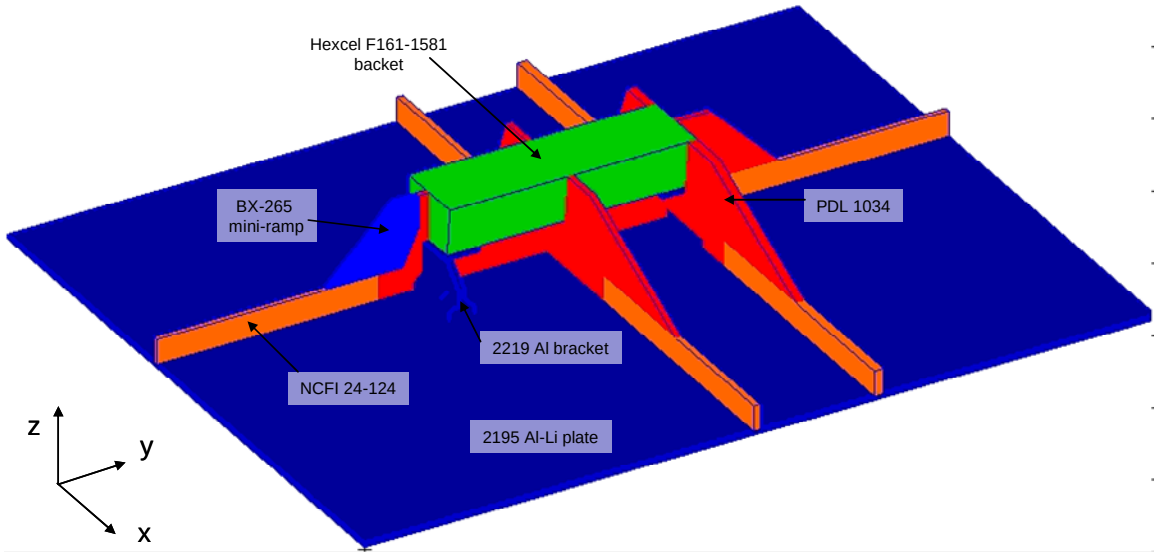

Figure 7.4-11. LO_2 Ramp Model Sections

The pressurized transversely isotropic NCFI 24-124 foam case is discussed here in detail as it is the most accurate physical representation and for the case with the highest stress levels. The normal stresses for this case are shown in Figures 7.4-12, 13, and 14. All three figures use the same fixed range scale for the stress level. Figures 7.4-15, 16, and 17 show the shear stresses. These three figures use their own fixed range scale for the stress level. The stress contour plots are plotted by material property meaning that stress results for the same material property are smoothed across element boundaries and stress results for elements adjacent to each other with different material properties are not. Thus, a discontinuity in the stress results indicates a material property interface.

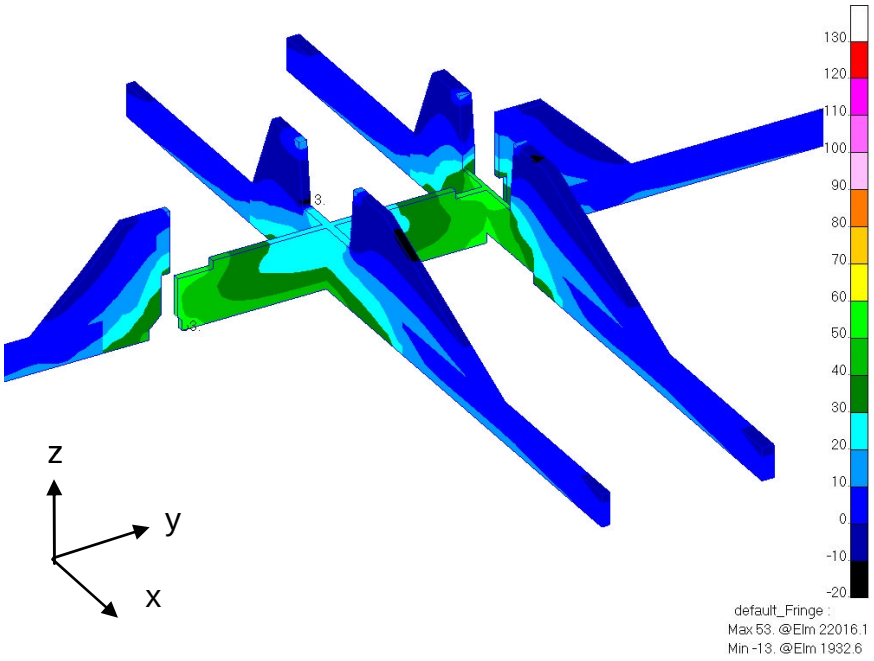

Figure 7.4-12. Foam σ_x in the LO_2 Ramp Model (units of psi)

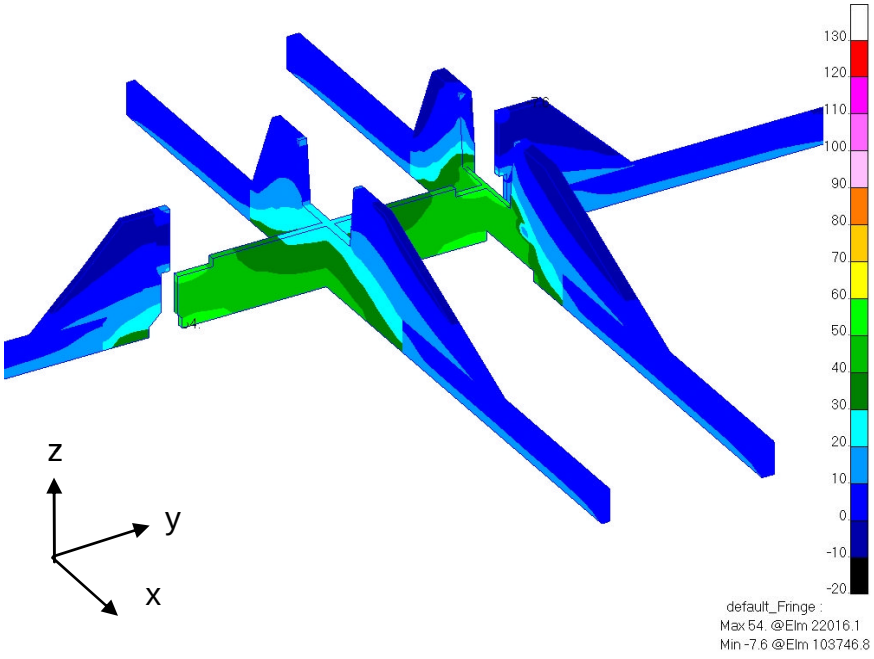

Figure 7.4.13. Foam σ_y in the LO_2 Ramp Model (units of psi)

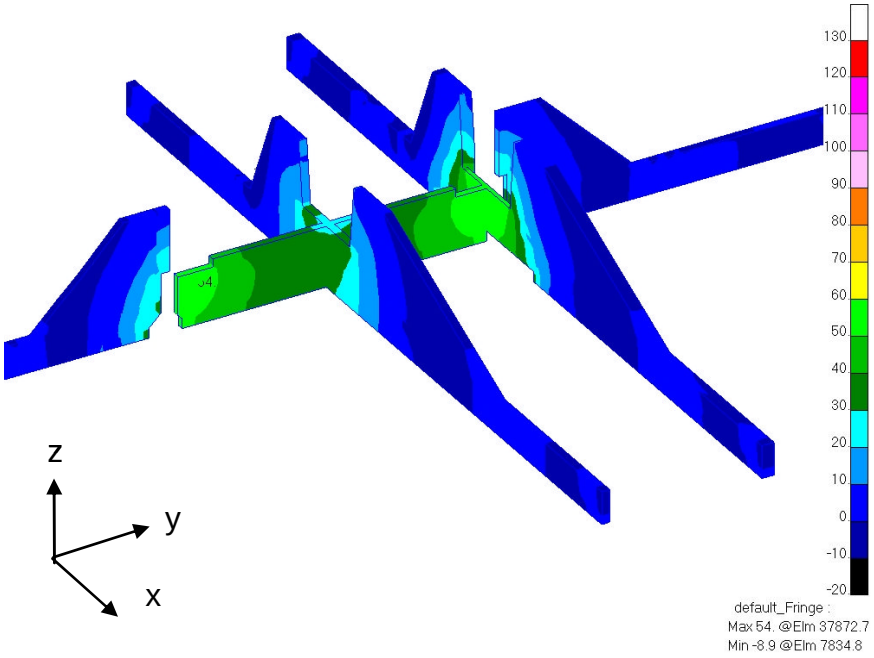

Figure 7.4-14. Foam σ_z in the LO_2 Ramp Model (units of psi)

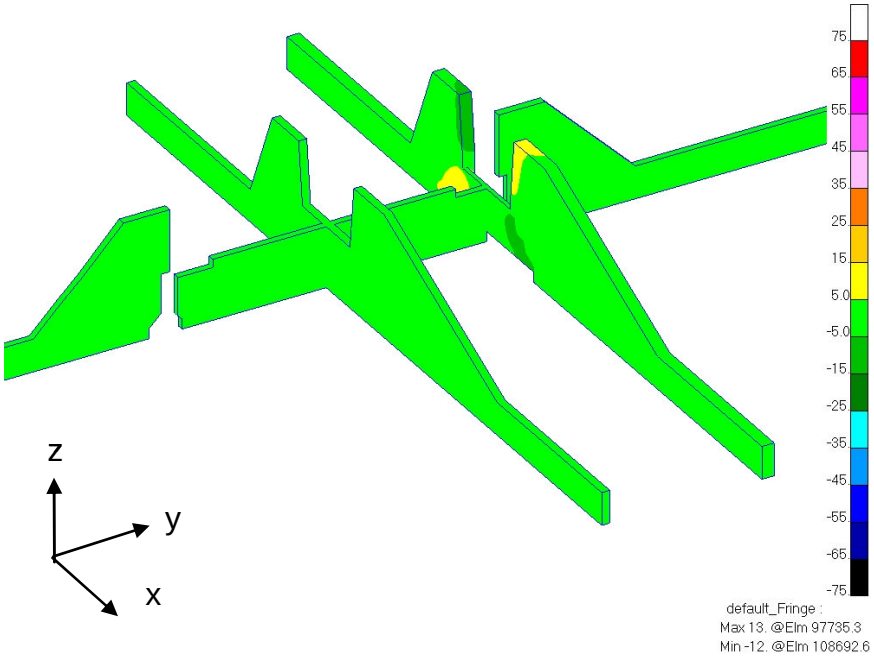

Figure 7.4-15. Foam τ_{xy} in the LO_2 Ramp Model (units of psi)

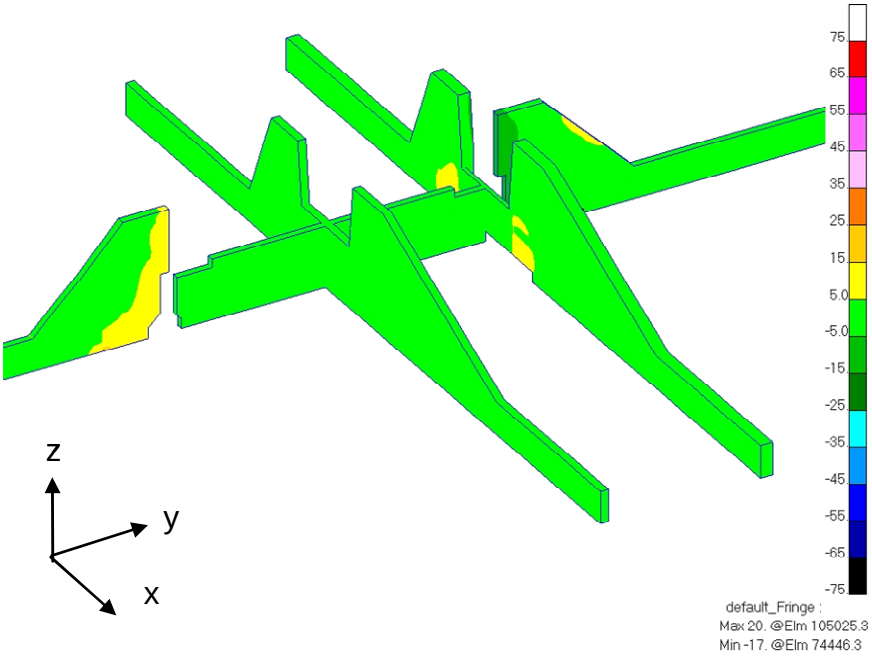

Figure 7.4-16. Foam τ_{yz} in the LO_2 Ramp Model (units of psi)

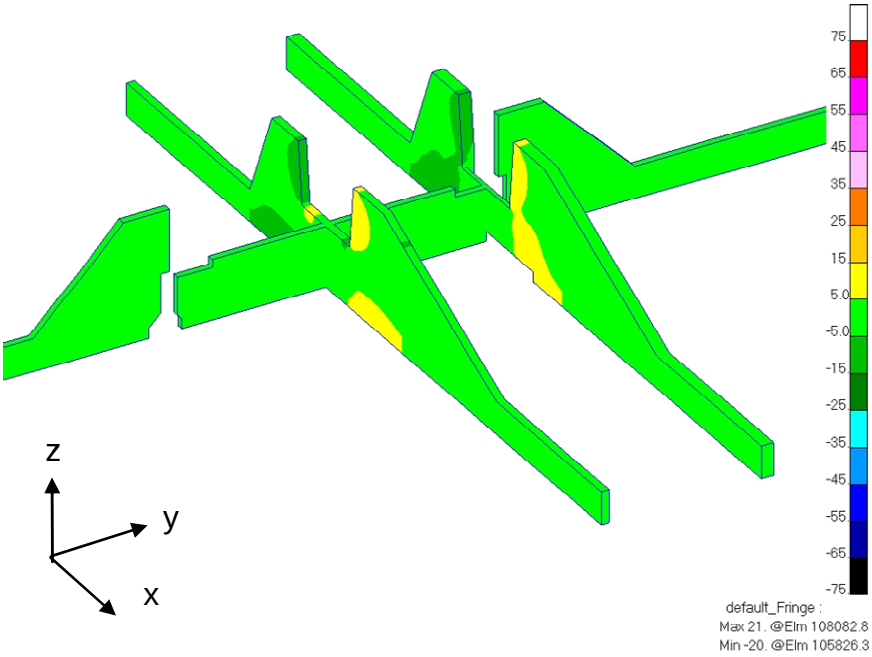

Figure 7.4-17. Foam τ_{zx} in the LO_2 Ramp Model (units of psi)

The stresses in the BX-265 foam mini-ramp and the surrounding PDL 1034 foam along the circumferential plane cut through the centerline of the bracket are shown in Figure 7.4-18, as are the material locations. The shear stresses along the same plane are shown in Figure 7.4-19.

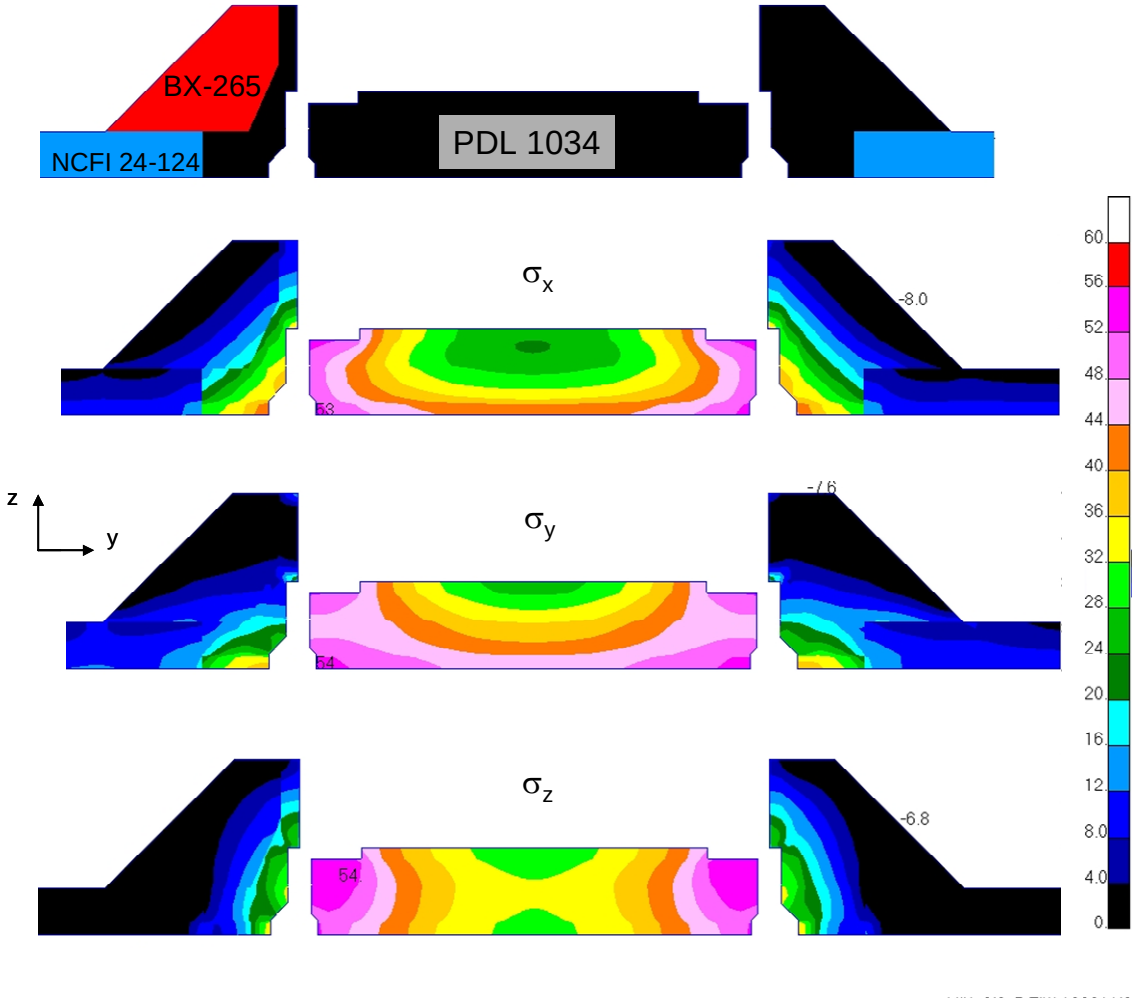

Figure 7.4-18. Foam Normal Stresses in the LO_2 Ramp Model (units of psi)

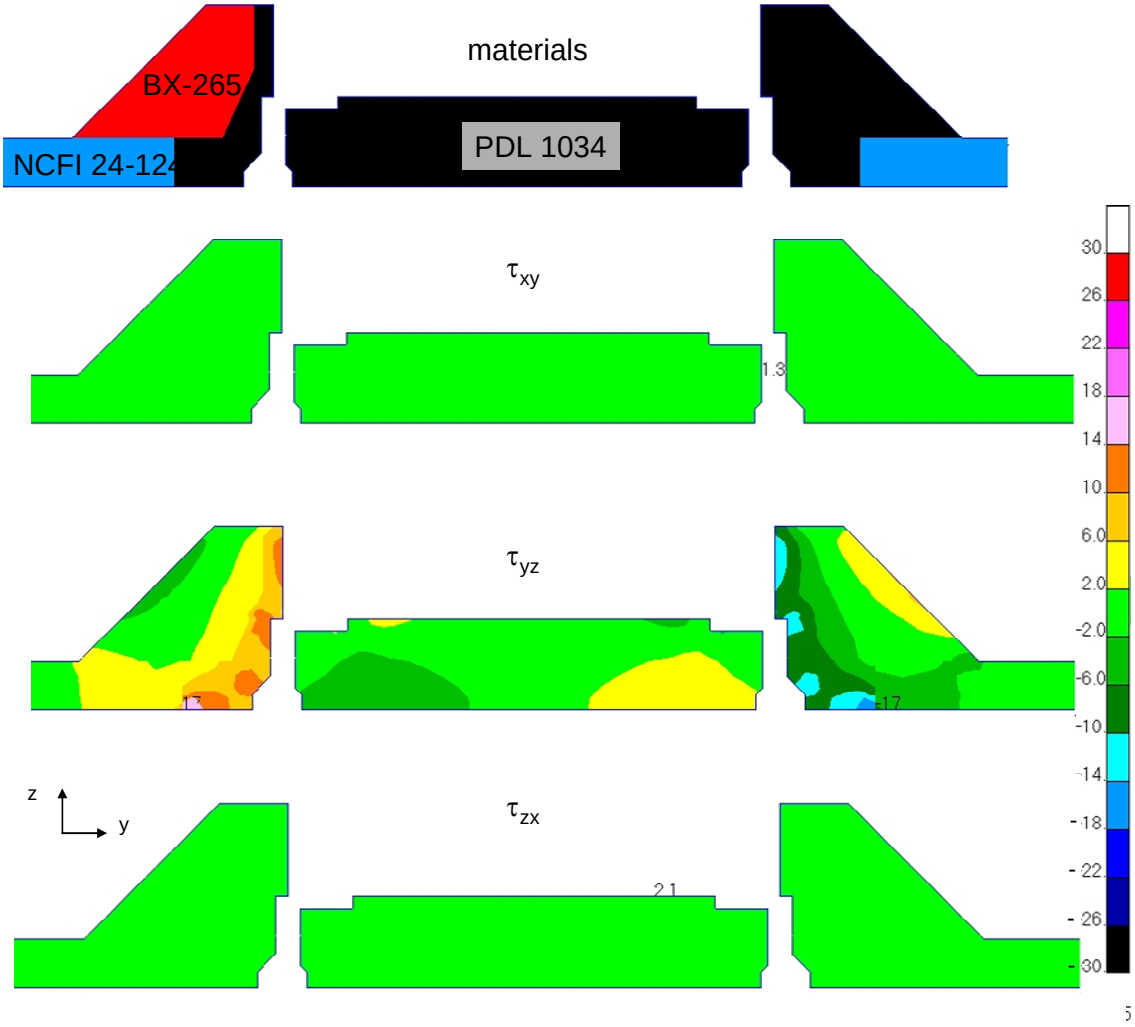

Figure 7.4-19. Foam Shear Stresses in the LO_2 Ramp Model (units of psi)

A comparison of the stresses in the left and right sides of the model shows that the BX-265 foam mini-ramp does not increase the stress in the PDL 1034 foam IFR beyond the levels seen where the mini-ramp region is filled by the PDL 1034 foam (i.e., where there was no PAL ramp to be removed and replaced by the mini-ramps). Also, comparing the stresses in the BX-265 foam mini-ramp to those calculated for the BX-265 foam Bipod closeout show that the stresses in the mini-ramp are no more than half of the highest values in the Bipod closeout. The LO_2 mini-ramps themselves are not severely stressed and they do not increase the stress in the existing PDL 1034 foam IFRs.

The stresses in the foam calculated along the section cut axially through the bracket mount are shown in Figures 7.4-20 and 7.4-21. Figure 7.4-20 shows the normal stresses and indicates the material layout. Figure 7.4-21 shows the foam shear stresses.

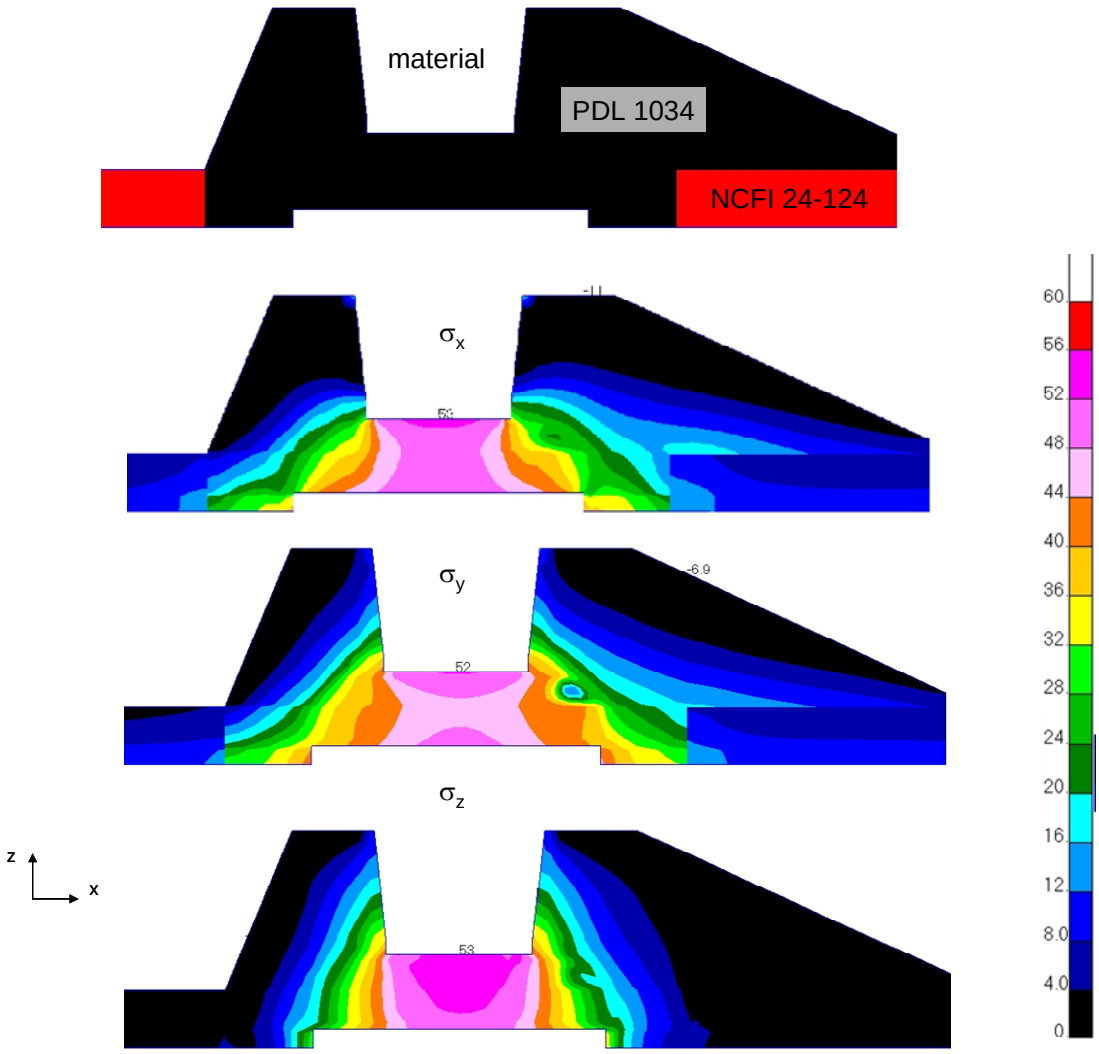

Figure 7.4-20. Foam Normal Stresses in the LO_2 Ramp Model (units of psi)

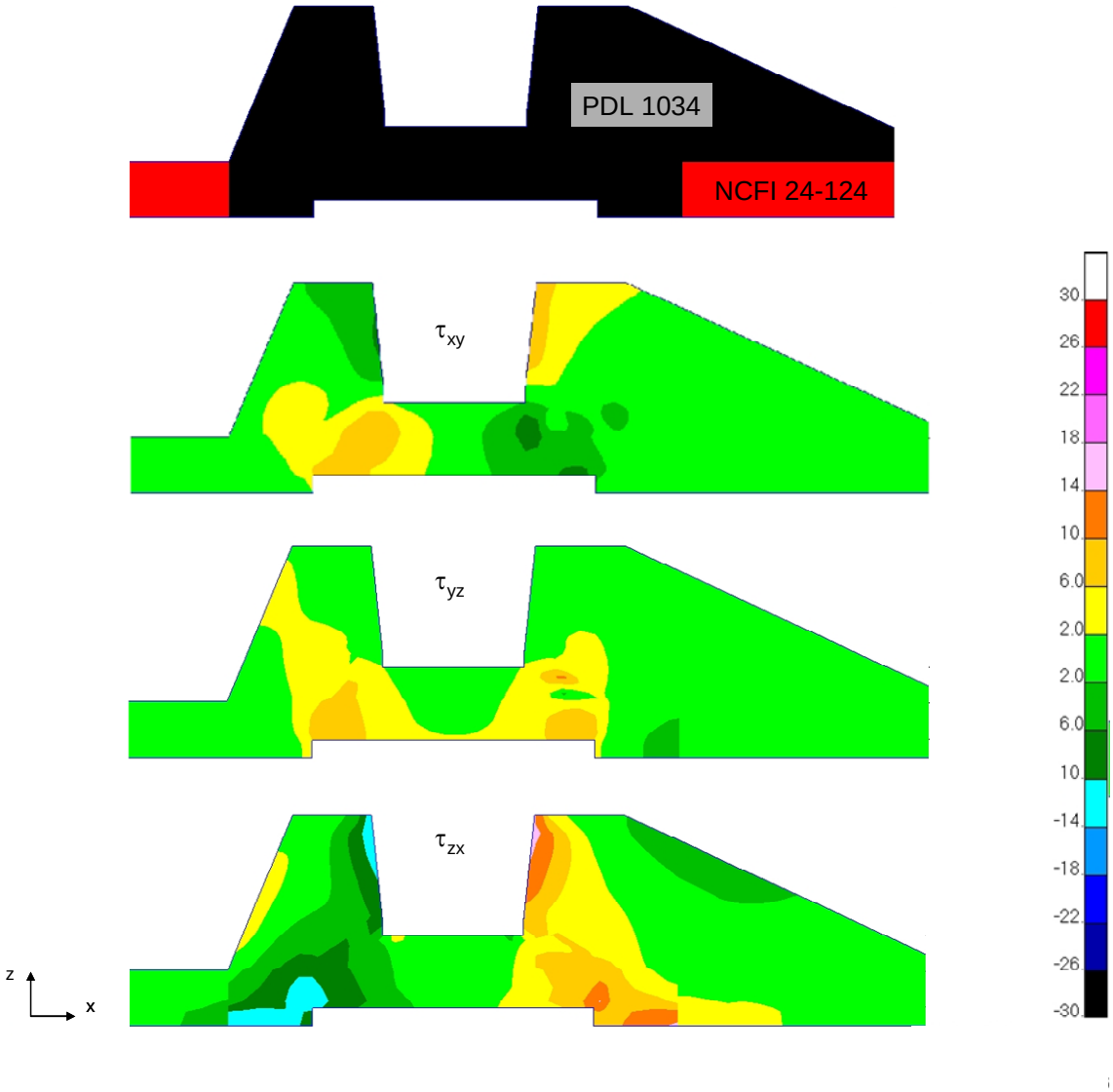

Figure 7.4-21. Foam Shear Stresses in the LO_2 Ramp Model (units of psi)

Figures 7.4-18 to 21 show that the stresses in the NCFI 24-124 foam are highest at the NCFI 24-124/PDL 1034/tank wall interface under the IFR.

LH_2 IFR Model

Five cases were run using the LH_2 IFR model. They were:

- isotropic properties for all materials – cold case

  - 25 psig tank pressure[20]
- transversely isotropic properties for NCFI 24-124 foam, isotropic properties for all other materials – cold case
  - zero tank pressure
  - 25 psig tank pressure
- transversely isotropic properties for NCFI 24-124 foam, isotropic properties for all other materials – hot case
  - zero tank pressure
  - 25 psig tank pressure

The pressure induced stresses on the substrate boundary at 25 psig were calculated based on the detailed dimensions of the tank wall and internal isogrid. First, equivalent tank thicknesses in the axial and circumferential directions were calculated. Those thicknesses were then used to calculate axial and hoop pressurization stresses in the tank wall to be applied to the appropriate model boundaries[21].

Figure 7.4-22 shows three sections that were cut through the model to facilitate presentation of the results. One section was cut along the circumferential plane through the center of the bracket. Two other sections were cut axially through the model, one through the model center and the other through the bracket mount. The figure shows the model baseplate, the phenolic insulators, the bracketry, and three types of foam. The BX-265 foam mini-ramp is on the left of the figure.

[20] The hydrogen tank is pressurized to 25 psig before loading. The less than 1 psi of LH_2 hydrostatic head at this location is neglected in the analysis as it is within the variation of the tank pressurization.
[21] At Station 1270 the effective circumferential thickness is 0.117 inches and the effective axial thickness is 0.137 inches. The hoop stress owing to 25 psig on the 13.8 ft radius tank is 35,400 psi. The axial stress for the same condition is 15,100 psi.

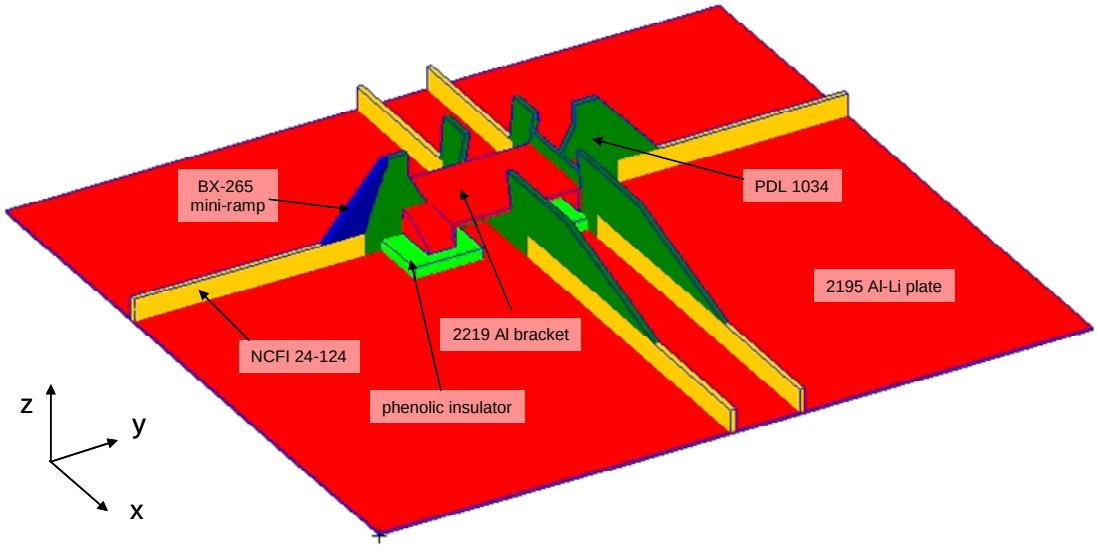

Figure 7.4-22. LH_2 Ramp Model Sections

The pressurized transversely isotropic NCFI 24-124 foam cold case is discussed here in detail as it is the most accurate physical representation for the case with the highest stress levels. The normal stresses in the foam are shown in Figures 7.4-23, 24, and 25. These three figures use the same fixed range scale for the stress level. Figures 7.4-26, 27, and 28 show the foam shear stresses. All three figures use the same fixed range scale for the stress level. The fixed ranges for these LH_2 plots are the same ranges as were used in the analogous LO_2 IFR plots. The stress contour plots are plotted by material property meaning that stress results for the same material property are smoothed across element boundaries and stress results for elements adjacent to each other with different material properties are not. Thus, a discontinuity in the stress results indicates a material property interface.

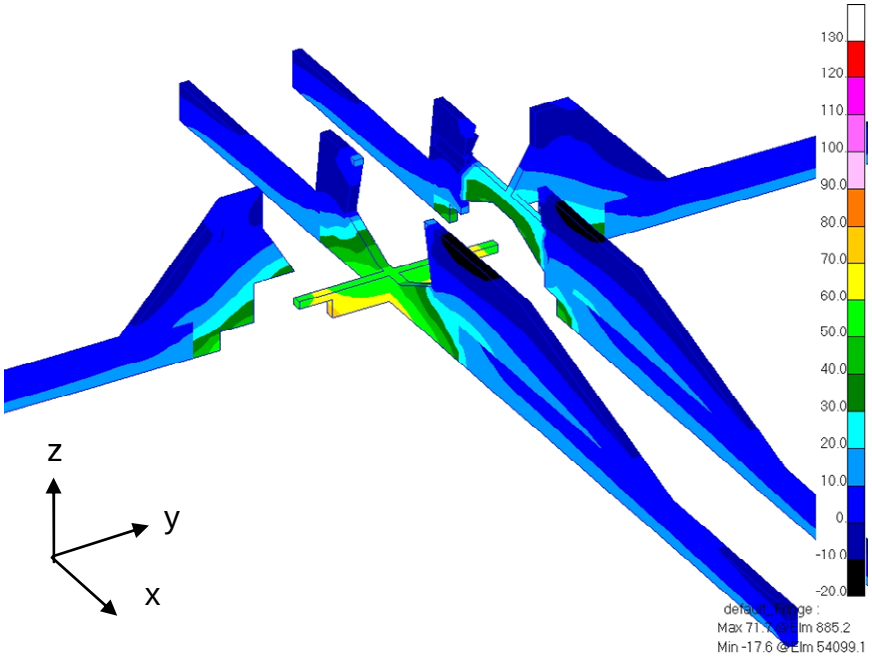

Figure 7.4-23. σ_x in the LH_2 Ramp Model (units of psi)

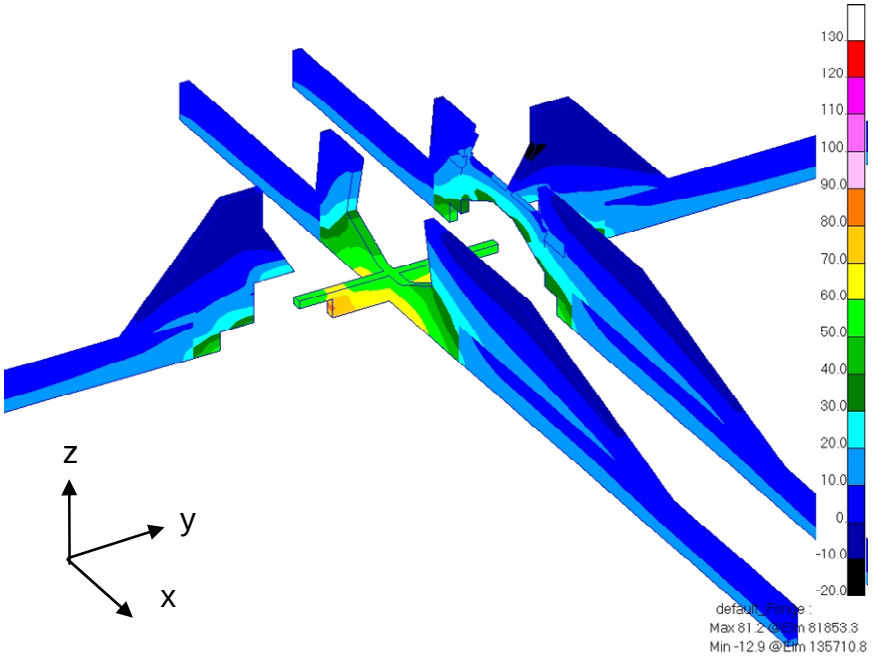

Figure 7.4.24. σ_y in the LH_2 Ramp Model (units of psi)

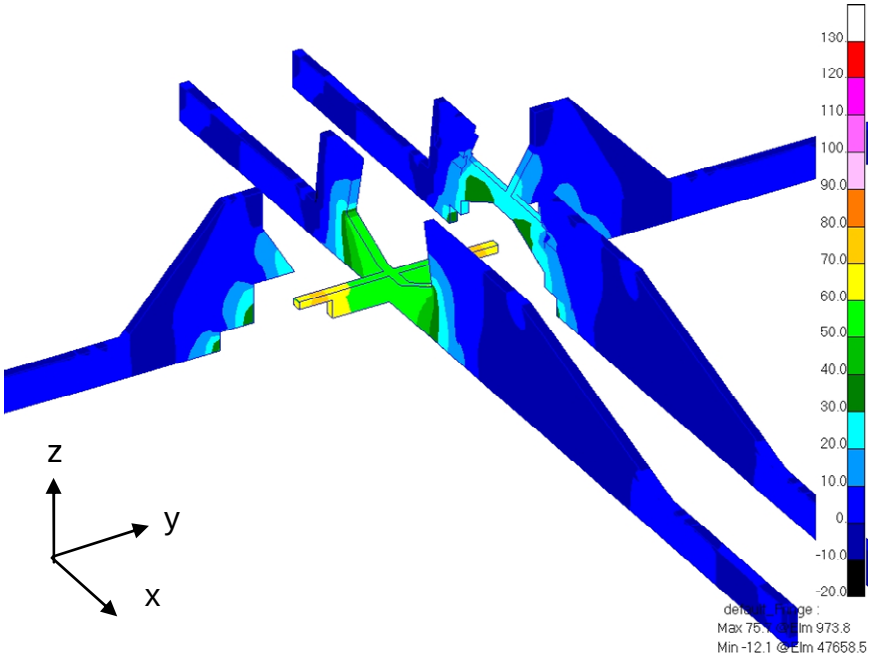

Figure 7.4-25. σ_z in the LH_2 Ramp Model (units of psi)

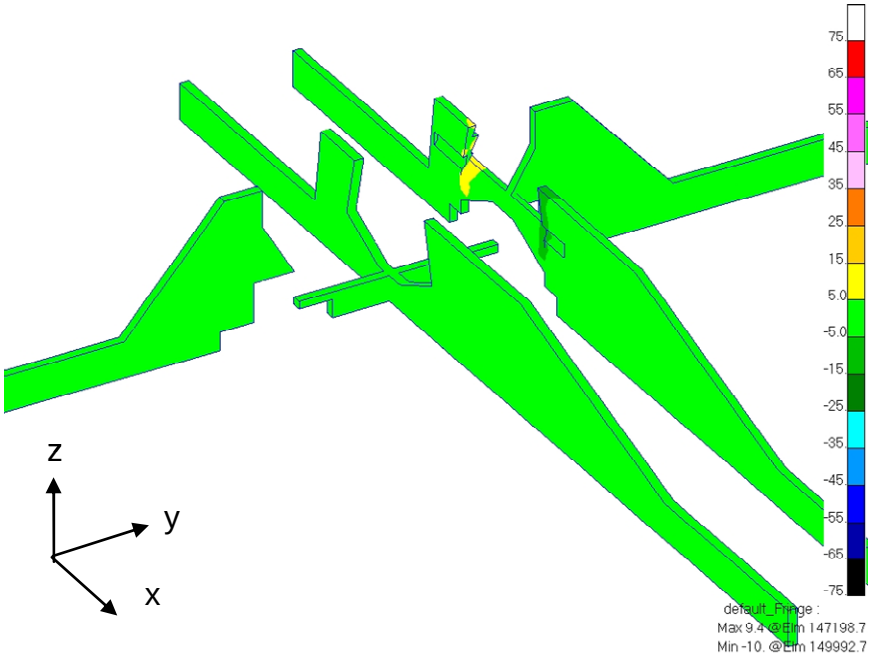

Figure 7.4-26. τ_{xy} in the LH_2 Ramp Model (units of psi)

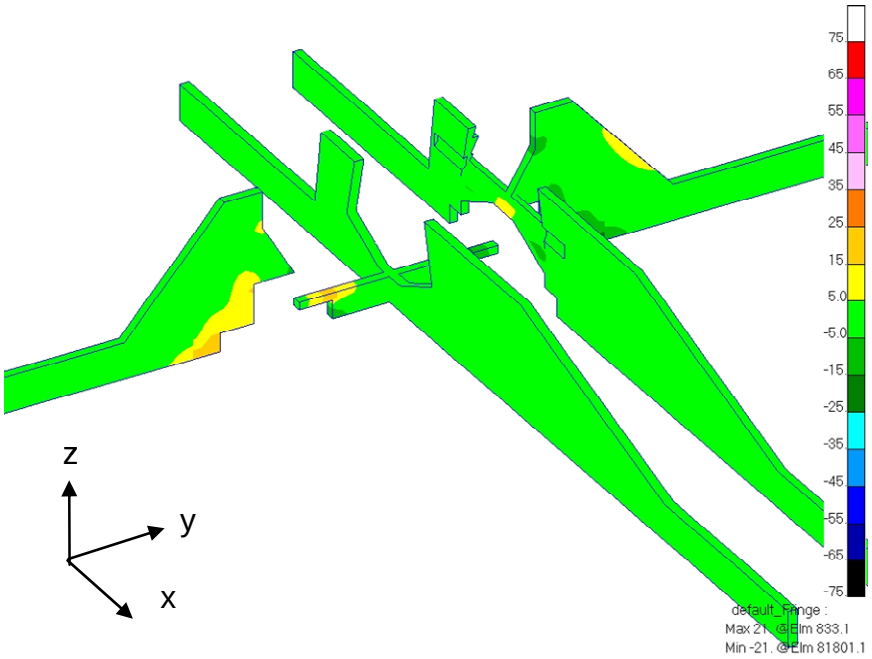

Figure 7.4-27. τ_{yz} in the LH_2 Ramp Model (units of psi)

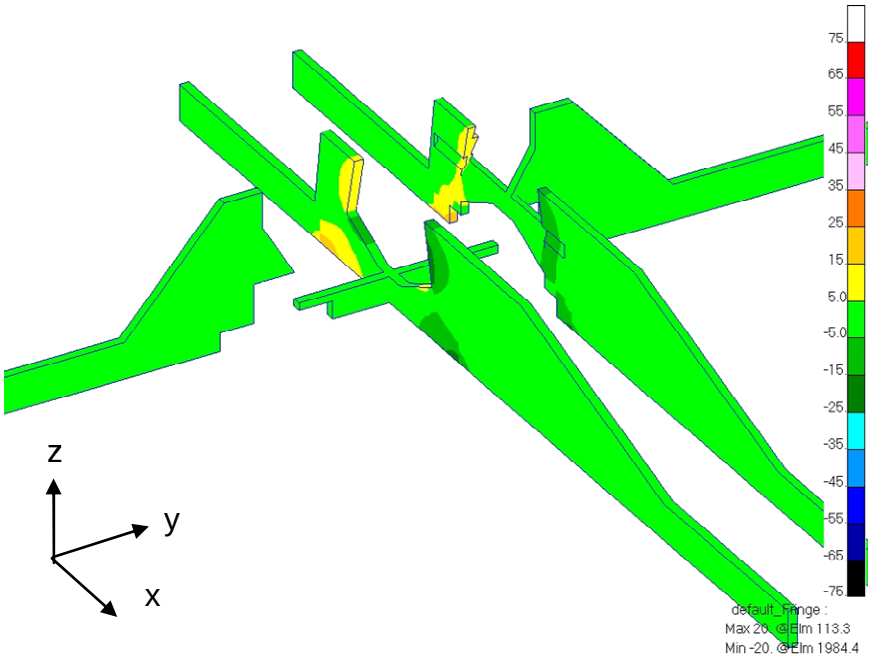

Figure 7.4-28. τ_{zx} in the LH_2 Ramp Model (units of psi)

The stresses in the BX-265 foam mini-ramp, surrounding PDL 1034 foam, and NCFI 24-124 foam along the circumferential plane cut through the centerline of the bracket are shown in Figure 7.4-30, as is the material layout. The foam shear stresses along the same plane are shown in Figure 7.4-31.

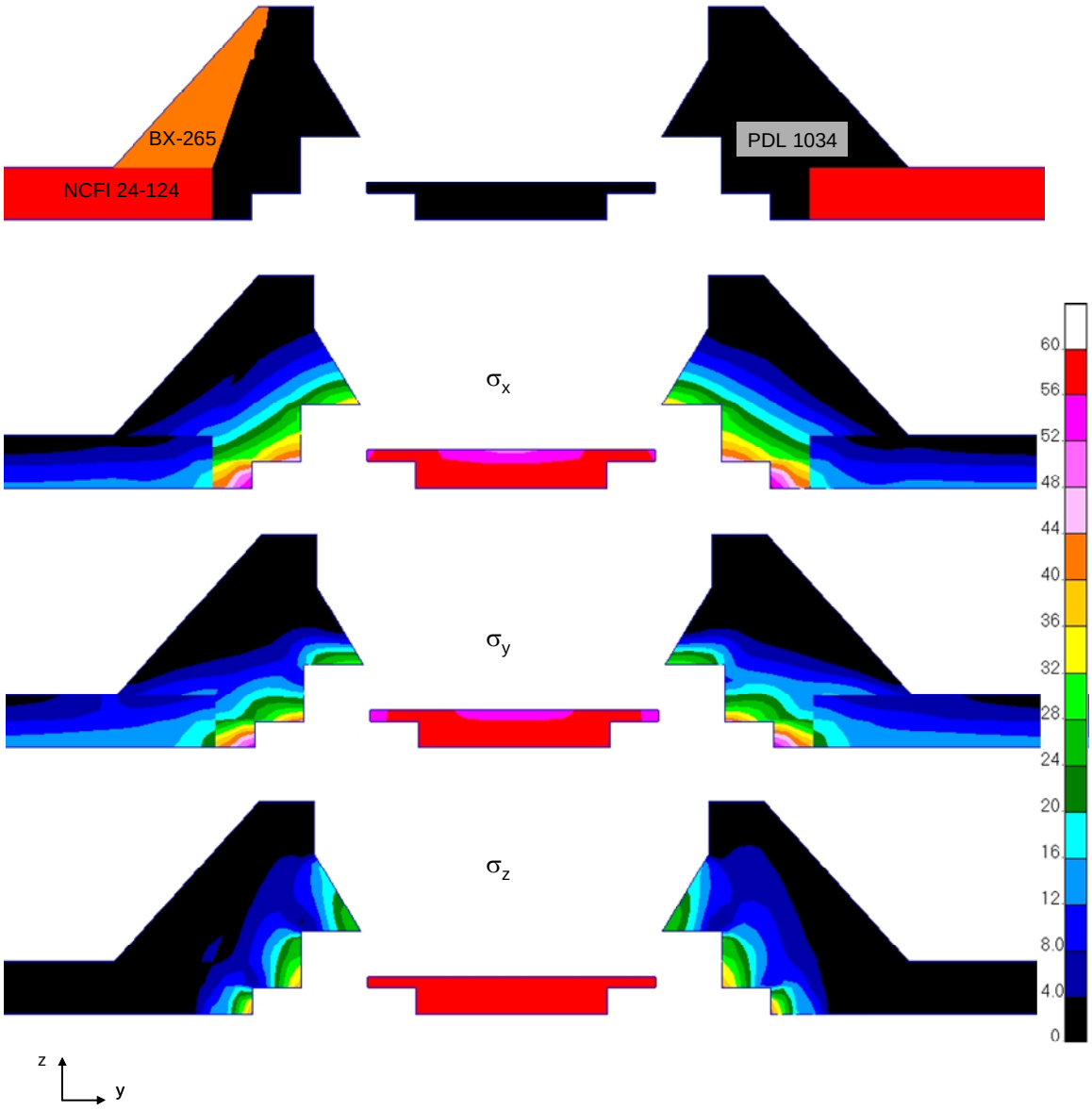

Figure 7.4-30. Normal Stresses in the LH_2 Ramp Model (units of psi)

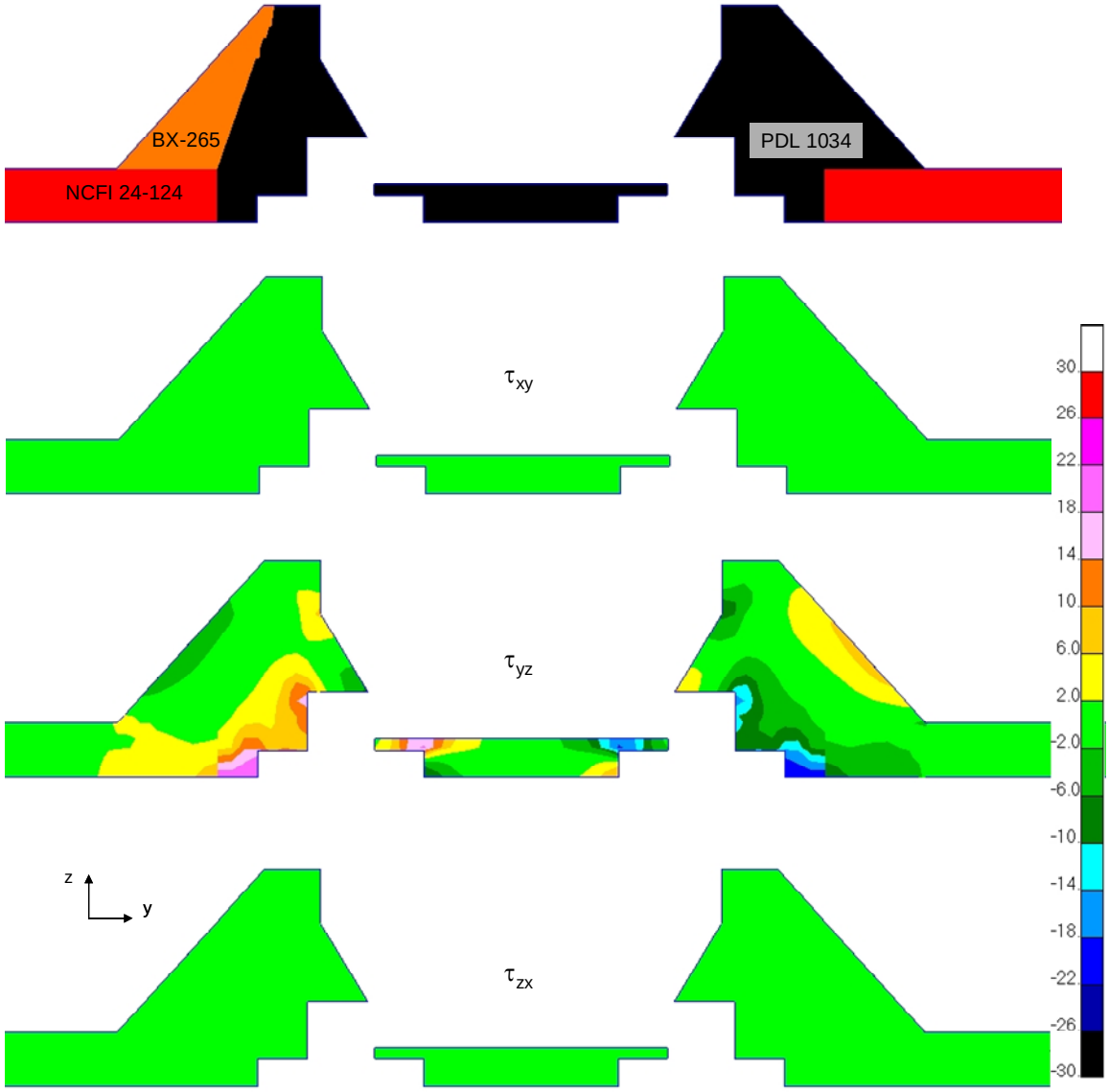

Figure 7.4-31. Shear Stresses in the LH_2 Ramp Model (units of psi)

A comparison of the stresses in the left and right sides of the model shows similar results to the LO_2 IFR model. The BX-265 foam mini-ramp does not increase the stress in the PDL 1034 foam IFR beyond the levels seen where the mini-ramp region is filled by the PDL 1034 foam (i.e., where there was no PAL ramp to be removed and replaced by the mini-ramps). Also, comparing the stresses in the BX-265 foam mini-ramp to those calculated for the BX-265 foam

Bipod closeout show that the stresses in the mini-ramp are no more than half of the highest values in the Bipod closeout. The LH_2 mini-ramps themselves are not severely stressed and they do not increase the stress in the existing PDL 1034 foam IFRs.

The stresses calculated along the section cut axially through the bracket mount are shown in Figures 7.4-32 and 7.4-33. Figure 7.4-32 shows the normal stresses and indicates the material layout. Figure 7.4-33 shows the shear stresses.

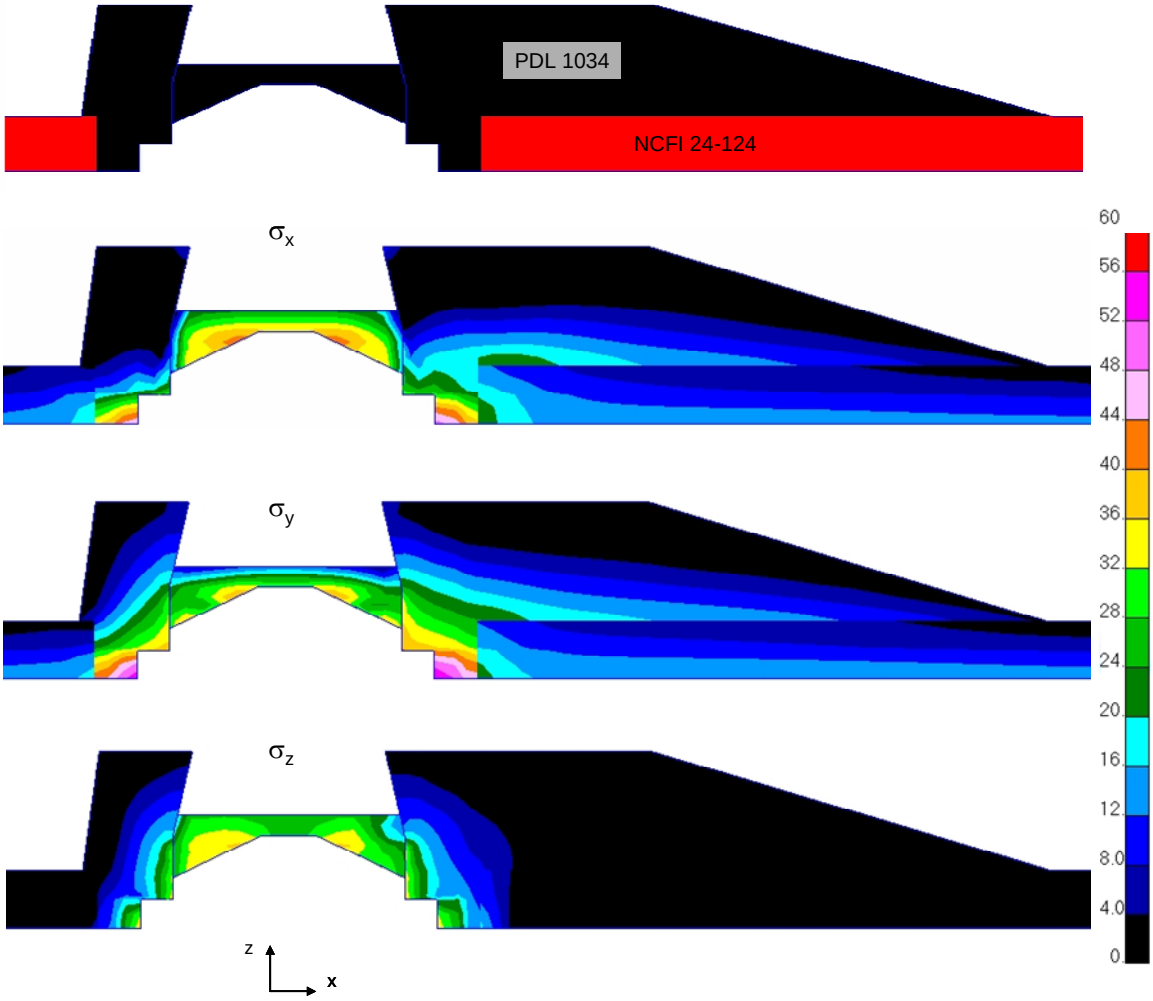

Figure 7.4-32. Normal Stresses in the LH_2 Ramp Model (units of psi)

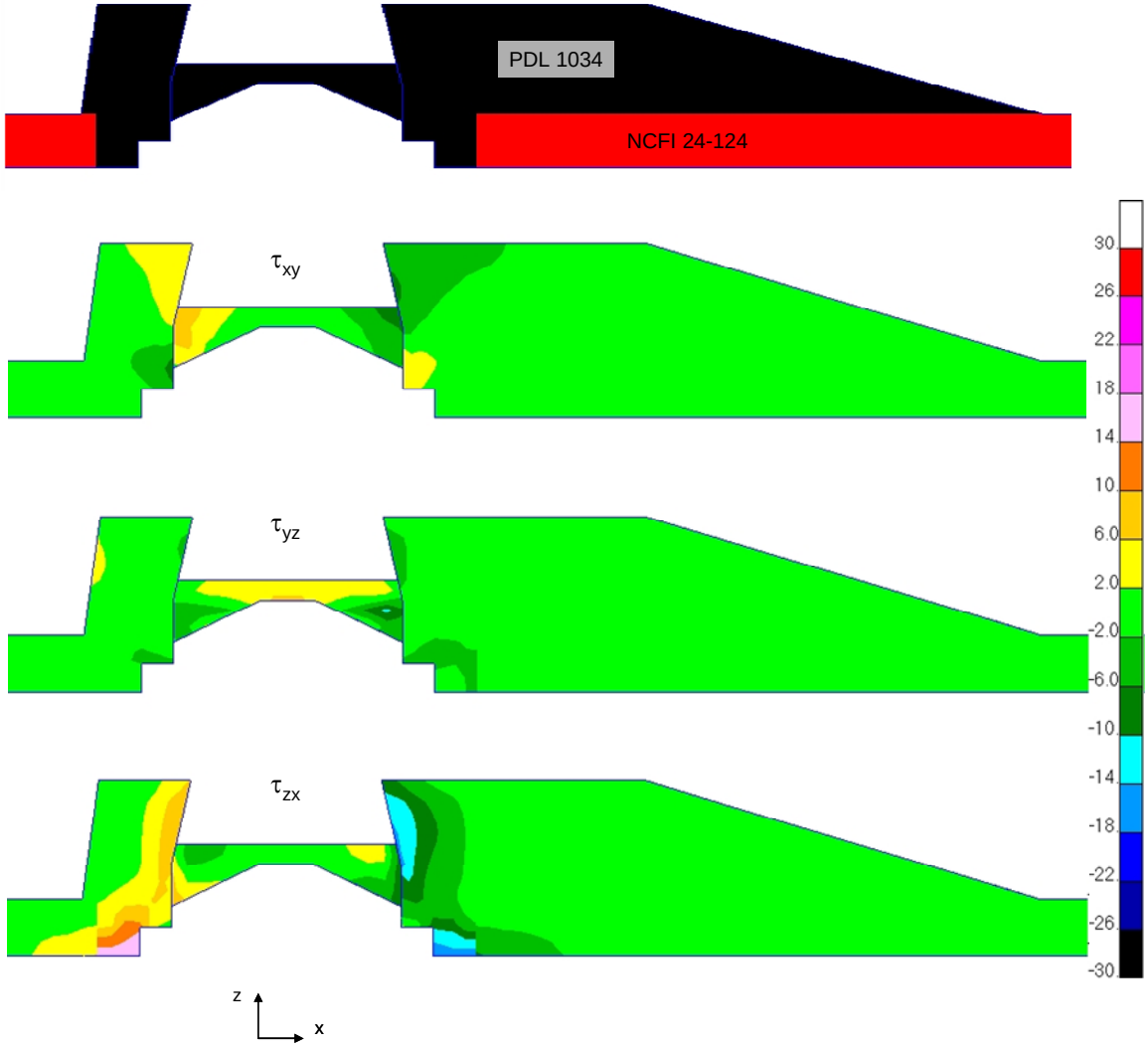

Figure 7.4-33. Shear Stresses in the LH_2 Ramp Model (units of psi)

As was observed for the LO_2 IFR, the stresses in the NCFI 24-124 foam are highest at the NCFI 24-124/PDL 1034/tank wall interface under the IFR. However, the stresses in the LH_2 NCFI 24-124 foam are higher than in the LO_2 IFR. In particular, the transverse shear stresses known to be associated with the formation of delaminations in laminated structures (τ_{zx} and τ_{yz}) are large. The level of stress in the NCFI 24-124 deep under the IFR are consistent with the dissections of IFRs on ET-120, which had been tanked twice. Two of the three LH_2 IFRs that were in locations with no PAL ramp (and are encompassed by these results) had cracks in the

NCFI 24-124 foam emanating from the rounded corners of the pocket as shown in Figure 7.4-34[22]. No cracks were found in any of the three LO_2 IFRs that were dissected.

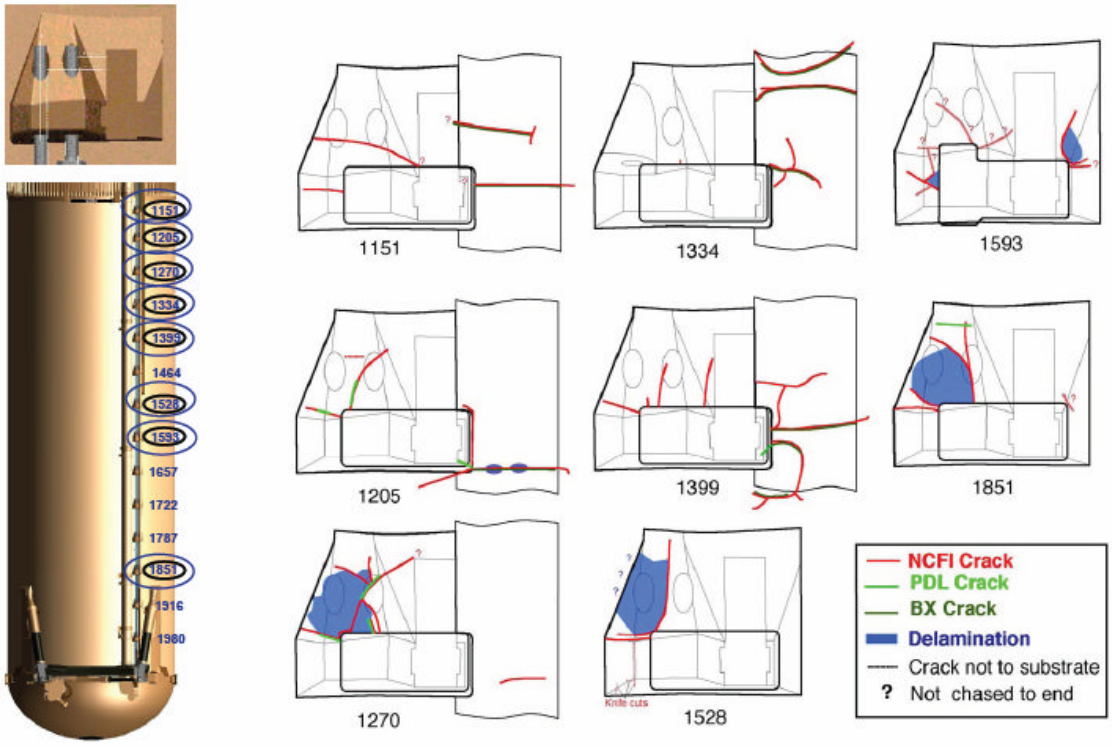

Figure 7.4-34. ET-120 LH_2 Ice/Frost Ramp Dissection Results

[22] ET-120 Dissection Collector Report 809-9440 Rev B, Lockheed-Martin Michoud Space Systems

8.0 Findings, Recommendations, and Observations

Thermal and stress analysis models were built to assess the thermally induced stresses in the ET Bipod closeout, plus the LO_2 and LH_2 Ice/Frost ramps. Models with various levels of detail ranging from simple geometric shapes to complete three-dimensional models were built that included the foam plus underlying structure and bracketry. Thermal analyses were used to generate steady-state temperature profiles, which were input as temperature distributions on the structural models. Based on these linear analysis models and associated assumptions related to geometry, materials and loadings, the following findings, recommendations, and observations are offered.

8.1 Findings

Bipod Models

F-1. An area of high stress on the Bipod axial centerline was found along the aluminum tank wall near the phenolic insulator. High stresses were also found along the phenolic insulator. A more complete assessment of stresses in the closeout requires a model that captures the three-dimensional effects in the closeout. *Section 7.2.1.*

F-2. There is a small region of slightly increased stress in the NCFI 24-124 foam near its joint with the Bipod closeout BX-265 foam. However, the presence of the interface does not substantially increase the thermally induced stress levels in the foam. *Section 7.2.2.*

LH_2 IFR Precursor Models

F-3. Removing the forward portion ("toe") of the LH_2 PDL 1034 IFRs, leaving only the NCFI 24-124 acreage foam, would reduce the thermally induced stresses in the NCFI 24-124 foam. However, the degree of reduction in the stresses cannot be accurately quantified from these models owing to their highly simplified configuration. *Section 7.3.*

LO_2 IFR Model

F-4. The LO_2 IFR BX-265 foam mini-ramp does not increase the stress in the PDL 1034 foam IFR beyond the levels seen where the mini-ramp region is filled by the PDL 1034 foam (i.e., where there was no PAL ramp to be removed and replaced by the mini-ramps). *Section 7.4.4*

F-5. The highest stresses in the LO_2 IFR BX-265 foam mini-ramp are less than half the extreme values in the Bipod closeout. Thus, the mini-ramp is not severely stressed. *Section 7.4.4*

LH_2 IFR Model

F-6. The LH_2 IFR BX-265 foam mini-ramp does not increase the stress in the PDL 1034 foam IFR beyond the levels seen where the mini-ramp region is filled by the PDL 1034 foam (i.e., where there was no PAL ramp to be removed and replaced by the mini-ramps). *Section 7.4.4*

F-7. The highest stresses in the LH_2 IFR BX-265 foam mini-ramp are less than half the extreme values in the Bipod closeout. The mini-ramp is not highly stressed. *Section 7.4.4*

F-8. The calculated stresses in the NCFI 24-124 foam are highest at the NCFI 24-124/PDL 1034/tank wall interface under the LH_2 IFR as they are in the LO_2 IFR. However, the highest calculated stresses in the LH_2 NCFI 24-124 foam are higher than in similar locations in the LO_2 IFR. This finding is consistent with the dissection results of IFRs on ET-120, which had been loaded twice with cryogenic propellant. Two of the three dissected LH_2 IFRs that were in locations with no protuberance aerodynamic load (PAL) ramp had cracks in the highly stressed areas of the NCFI 24-124 foam outboard of the cable tray. No cracks were found in any of the three LO_2 IFRS that were dissected. *Section 7.4.4*

8.2 Recommendations

R-1. The analysis of the Bipod closeout indicated some areas of high thermally induced stress. A full three-dimensional Bipod closeout model with sufficient detail to more fully investigate thermally induced stresses has been developed by the ET Project. Preliminary stress results were obtained prior to STS-114 using a now-outdated foam mechanical property set. This model should be rerun using the most current understanding of the foam properties to allow accurate assessment of the stresses in the Bipod closeout. *F-1*

8.3 Observations

O-1. The IFR stress results of the present work are consistent with the results obtained by the ET Project using models with similar granularity. No further independent modeling of the thermally induced stresses in the IFRs is warranted.

9.0 Lessons Learned

There were no lessons learned during this consultation.

10.0 Definition of Terms

Corrective Actions	Changes to design processes, work instructions, workmanship practices, training, inspections, tests, procedures, specifications, drawings, tools, equipment, facilities, resources, or material that result in preventing, minimizing, or limiting the potential for recurrence of a problem.
Finding	A conclusion based on facts established during the assessment/inspection by the investigating authority.
Lessons Learned	Knowledge or understanding gained by experience. The experience may be positive, as in a successful test or mission, or negative, as in a mishap or failure. A lesson must be significant in that it has real or assumed impact on operations; valid in that it is factually and technically correct; and applicable in that it identifies a specific design, process, or decision that reduces or limits the potential for failures and mishaps, or reinforces a positive result.
Observation	A factor, event, or circumstance identified during the assessment/inspection that did not contribute to the problem, but if left uncorrected has the potential to cause a mishap, injury, or increase the severity should a mishap occur.
Problem	The subject of the technical assessment/inspection.
Requirement	An action developed by the assessment/inspection team to correct the cause or a deficiency identified during the investigation. The requirements will be used in the preparation of the corrective action plan.
Root Cause	Along a chain of events leading to a mishap or close call, the first causal action or failure to act that could have been controlled systemically either by policy/practice/procedure or individual adherence to policy/practice/procedure.

11.0 Alternate View Point

There were no alternate view points during this consultation.

12.0 List of Acronyms

Al	aluminum
Al-Li	aluminum-lithium
ET	External Tank
GRC	Glenn Research Center
HQ	Headquarters
IFR	Ice/Frost Ramp
JSC	Johnson Space Center
LaRC	Langley Research Center
LH_2	Liquid Hydrogen
LO_2	Liquid Oxygen
NASA	National Aeronautics and Space Administration
NCFI	North Carolina Foam Insulator
NESC	NASA Engineering and Safety Center
NRB	NESC Review Board
PAL	Protuberance Aerodynamic Load
PDL	Process Data Logging (FoamMix®)
PSIG	Pounds Per Square Inch Gage
SLA	Super Lightweight Ablator

Volume II: Appendices

A ITA/I Request Form (NESC-PR-003-FM-01)
B Foam Mechanical Properties

Appendix A. ITA/I Request Form (NESC-PR-003-FM-01)

NASA Engineering and Safety Center Request Form		
Submit this ITA/I Request, with associated artifacts attached, to: nrbexecsec@nasa.gov, or to NRB Executive Secretary, M/S 105, NASA Langley Research Center, Hampton, VA 23681		
Section 1: NESC Review Board (NRB) Executive Secretary Record of Receipt		
Received (mm/dd/yyyy h:mm am/pm) 2/1/2006 12:00 AM	Status: New	Reference #: 06-012-I
Initiator Name: Ralph Roe	E-mail: ralph.r.roe@nasa.gov	Center: NESC
Phone: (757)-864-2400, Ext ____	Mail Stop:	
Short Title: External Tank (ET) Foam Thermal Analysis Project		
Description: Team is assembled: One thermal analyst and one structural analyst Team will build simplified models (2-d where possible) to look at the hot spots for cracking. Simplified approach is doable and will yield accuracy in line with the (only available) assumption of foam as a linear elastic isotropic material.		
Source (e.g. email, phone call, posted on web): Announced at NESC Face-to-Face		
Type of Request: Assessment		
Proposed Need Date:		
Date forwarded to Systems Engineering Office (SEO): (mm/dd/yyyy h:mm am/pm):		
Section 2: Systems Engineering Office Screening		
Section 2.1 Potential ITA/I Identification		
Received by SEO: (mm/dd/yyyy h:mm am/pm): 2/17/2006 12:00 AM		
Potential ITA/I candidate? ☒ Yes ☐ No		
Assigned Initial Evaluator (IE): Approved out of board on 2/1/2004 at NESC F2F by Ralph Roe. Eugene Ungar to lead and present Plan		
Date assigned (mm/dd/yyyy): 2/21/2006		
Due date for ITA/I Screening (mm/dd/yyyy):		
Section 2.2 Non-ITA/I Action		
Requires additional NESC action (non-ITA/I)? ☐ Yes ☐ No		
If yes:		
Description of action:		
Actionee:		
Is follow-up required? ☐ Yes ☐ No If yes: Due Date:		
Follow-up status/date:		
If no:		
NESC Director Concurrence (signature):		
Request closure date:		

NESC Request Form
NESC-PR-003-FM-01, v1.0

Page 1 of 3

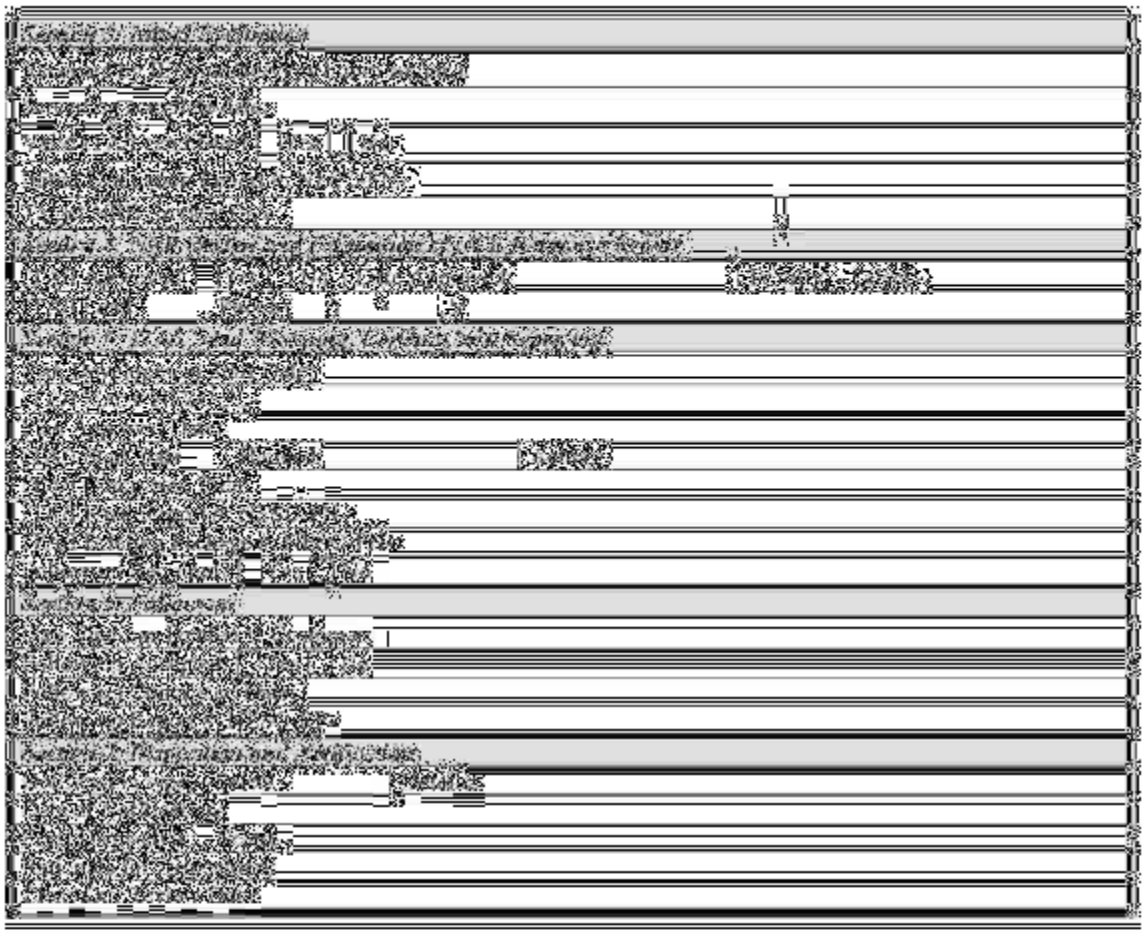

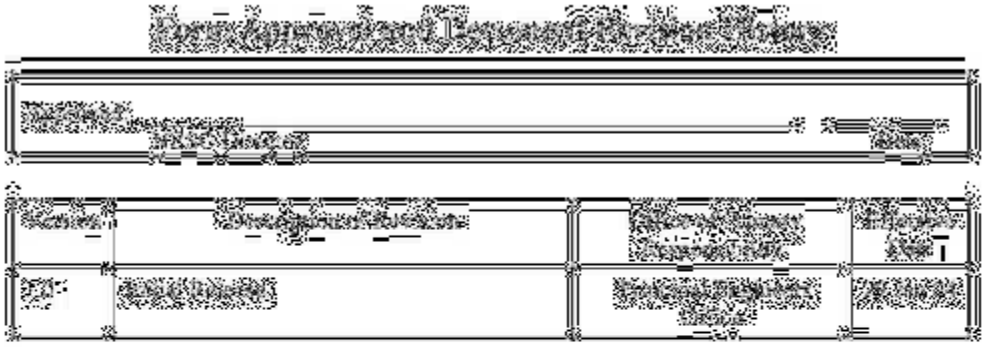

Appendix B. Foam Mechanical Properties

Table B-1. Isotropic Properties
E- Youngs modulus
ν – Poisson's ratio
α – coefficient of thermal expansion

BX-265 foam Manual				Solid
Temp (F)	E (psi)	ν		α (in/in/F)
-423	1600	0.30		3.31E-05
-320	1400	0.30		3.94E-05
-100	1038	0.30		5.47E-05
75	750	0.30		7.00E-05
200	271	0.30		1.35E-04
250	20	0.30		

NCFI 24-124 foam				Solid
Temp (F)	E (psi)	ν		α (in/in/F)
-423	1500	0.30		2.68E-05
-320	1292	0.30		3.32E-05
-100	937	0.30		3.40E-05
75	654	0.30		4.00E-05
200	479	0.30		4.90E-05
300	345	0.30		1.09E-04
450	20	0.30		

PDL 1034 foam				Solid
Temp (F)	E (psi)	ν		α (in/in/F)
-423	4062	0.30		2.66E-05
-320	3545	0.30		3.29E-05
-100	2428	0.30		4.12E-05
75	1540	0.30		5.00E-05
200	756	0.30		1.18E-04
300	141	0.30		3.01E-04
320	20	0.30		

Table B-2. Transversely Isotropic Properties

BX-265 Manual

Temp (F)	E11 (psi)	E22 (psi)	E33 (psi)	ν12	ν 21	ν 13	ν 31	ν 23	ν 32	G12 (psi)	G13 (psi)	G23 (psi)	α11 (in/in/F)	α22 (in/in/F)	α33 (in/in/F)
-423	1600	1600	4800	0.40	0.40	0.25	0.75	0.25	0.75	571	488	488	3.31E-05	2.91E-05	2.29E-05
-320	1400	1400	4200	0.40	0.40	0.25	0.75	0.25	0.75	500	427	427	3.94E-05	3.54E-05	2.81E-05
-100	1038	1038	3114	0.40	0.40	0.25	0.75	0.25	0.75	371	317	317	5.36E-05	4.79E-05	3.47E-05
75	750	750	2250	0.40	0.40	0.25	0.75	0.25	0.75	268	229	229	7.00E-05	6.00E-05	4.00E-05
200	271	271	813	0.40	0.40	0.25	0.75	0.25	0.75	97	83	83	1.35E-04	1.35E-04	9.69E-05
250	20	20	60	0.40	0.40	0.25	0.75	0.25	0.75	10	10	10			

NCFI 24-124

Temp (F)	E11 (psi)	E22 (psi)	E33 (psi)	ν 12	ν 21	ν 13	ν 31	ν 23	ν 32	G12 (psi)	G13 (psi)	G23 (psi)	α11 (in/in/F)	α22 (in/in/F)	α33 (in/in/F)
-423	1500	1500	6000	0.40	0.40	0.20	0.80	0.20	0.80	536	429	429	2.68E-05	2.68E-05	2.32E-05
-320	1292	1292	5168	0.40	0.40	0.20	0.80	0.20	0.80	461	369	369	3.32E-05	3.32E-05	2.85E-05
-100	937	937	3747	0.40	0.40	0.20	0.80	0.20	0.80	335	268	268	3.40E-05	3.40E-05	3.87E-05
75	654	654	2616	0.40	0.40	0.20	0.80	0.20	0.80	234	187	187	4.00E-05	4.00E-05	5.00E-05
200	479	479	1916	0.40	0.40	0.20	0.80	0.20	0.80	171	137	137	4.90E-05	4.90E-05	6.46E-05
300	345	345	1380	0.40	0.40	0.20	0.80	0.20	0.80	123	99	99	1.09E-04	1.09E-04	1.19E-04
450	20	20	80	0.40	0.40	0.20	0.80	0.20	0.80	10	10	10			

PDL-1034

Temp (F)	E11 (psi)	E22 (psi)	E33 (psi)	ν 12	ν 21	ν 13	ν 31	ν 23	ν 32	G12 (psi)	G13 (psi)	G23 (psi)	α11 (in/in/F)	α22 (in/in/F)	α33 (in/in/F)
-423	4062	4062	5971	0.42	0.42	0.38	0.56	0.38	0.56	1430	1401	1401	2.66E-05	2.66E-05	2.42E-05
-320	3545	3545	5211	0.42	0.42	0.38	0.56	0.38	0.56	1248	1223	1223	3.29E-05	3.29E-05	3.02E-05
-100	2428	2428	3570	0.42	0.42	0.38	0.56	0.38	0.56	855	838	838	4.12E-05	4.12E-05	3.80E-05
75	1540	1540	2264	0.42	0.42	0.38	0.56	0.38	0.56	542	531	531	5.00E-05	5.00E-05	5.00E-05
200	756	756	1111	0.42	0.42	0.38	0.56	0.38	0.56	266	261	261	1.18E-04	1.18E-04	1.28E-04
300	141	141	207	0.42	0.42	0.38	0.56	0.38	0.56	50	49	49	3.01E-04	3.01E-04	3.55E-04
320	20	20	29	0.42	0.42	0.38	0.56	0.38	0.56	10	10	10			

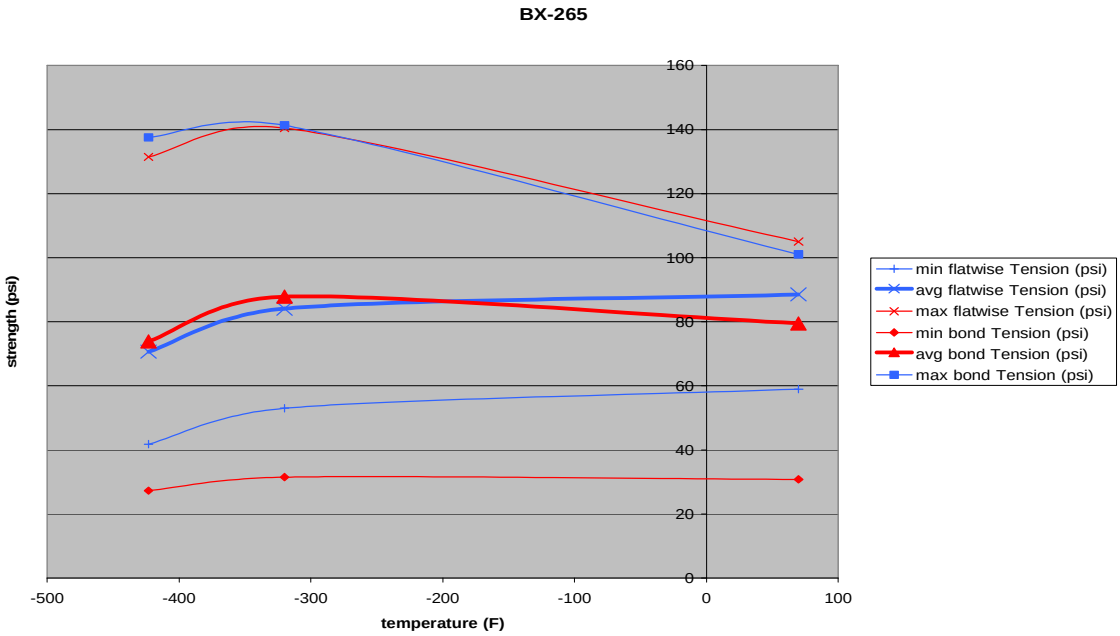

Figure B-1. BX-265 foam Tensile Strength

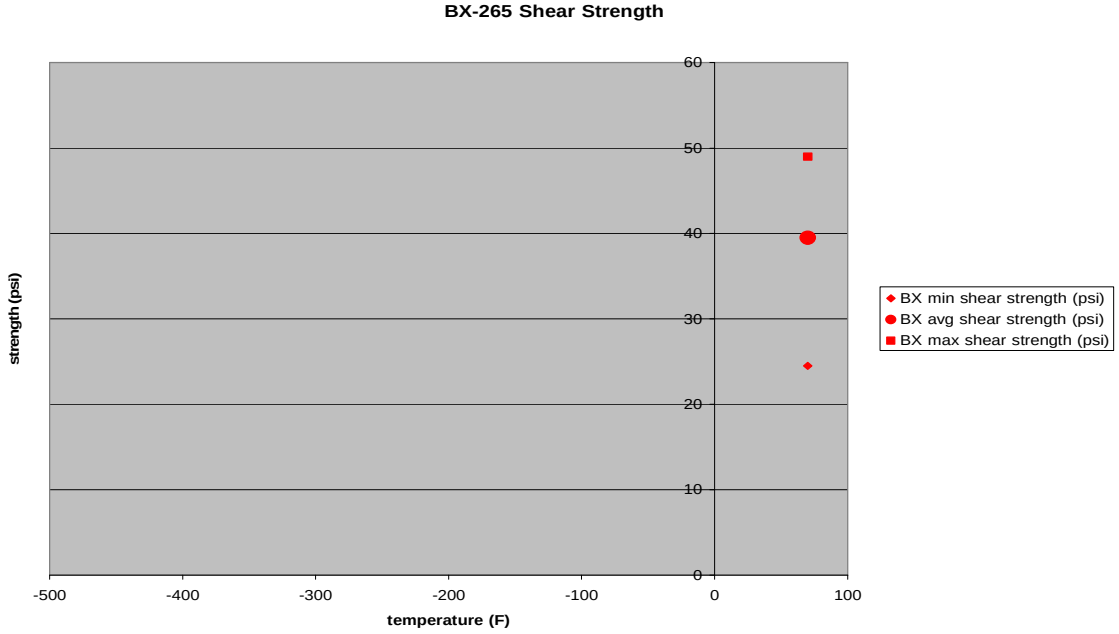

Figure B-2. BX-265 foam Shear Strength

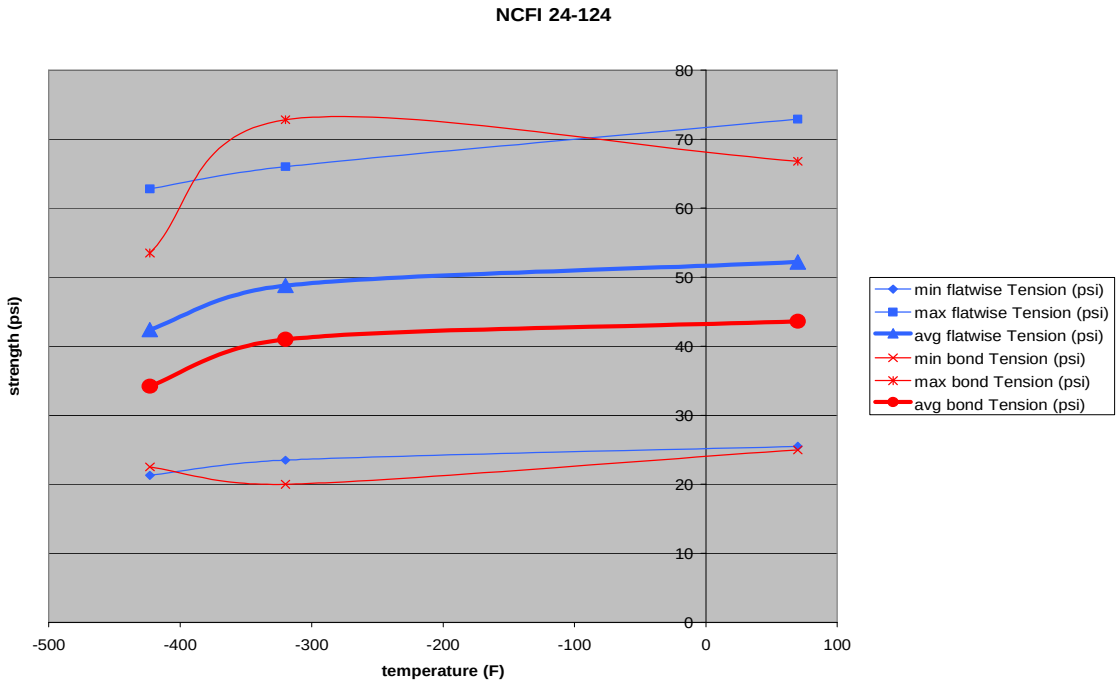

Figure B-3 – NCFI 24-124 foam Tensile Strength

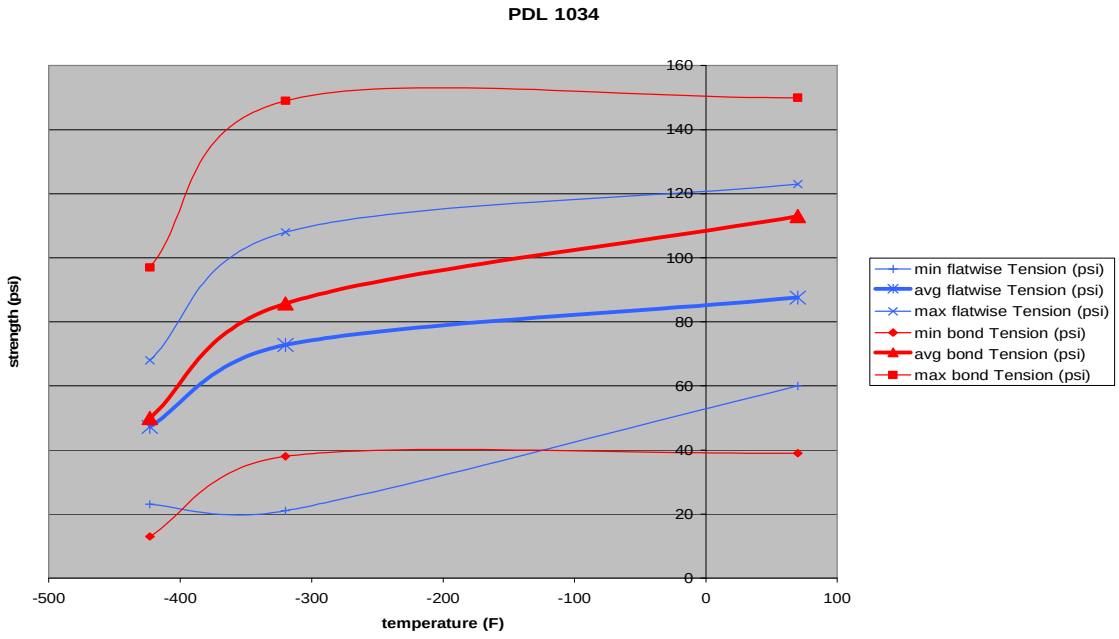

Figure B-4 – NCFI 24-124 foam Shear Strength

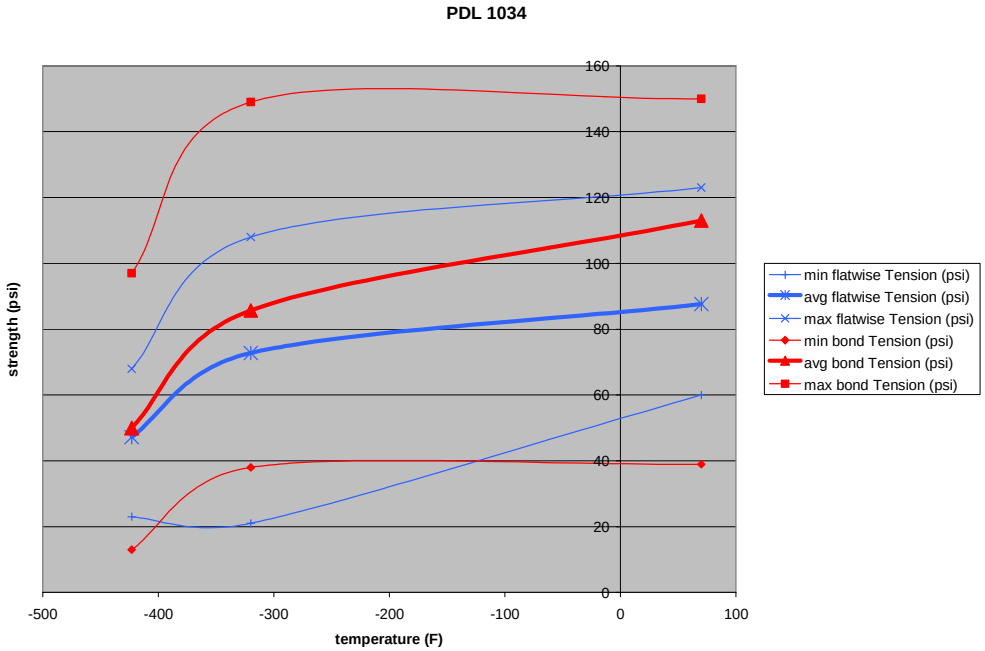

Figure B-5. PDL 1034 foam Tensile Strength

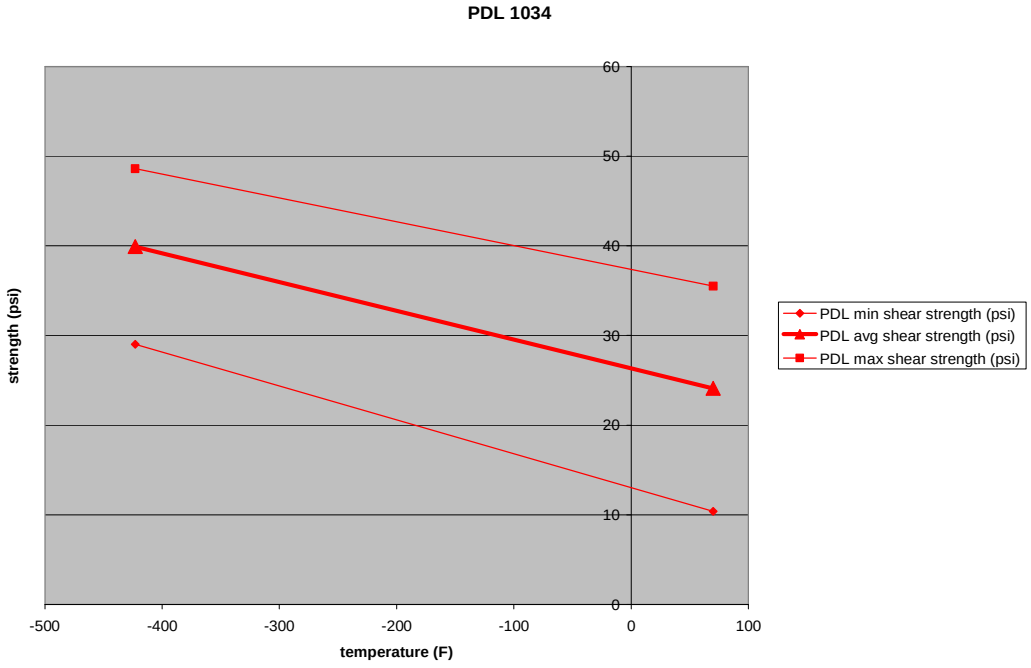

Figure B-6. PDL 1034 foam Shear Strength

Approval and Document Revision History

Approved:	Original signed on file	8-7-06
	NESC Director	Date

Version	Description of Revision	Office of Primary Responsibility	Effective Date
1.0	Initial Release	NESC Principal Engineer's Office	7-27-06